sections were double-stained with a combination of a goat antimouse serum albumin antibody (Abcam) and a rabbit anti-GFP antibody followed by the secondary antibody and development as described above. To quantify fibrosis, paraffin-embedded sections were stained with Azan and viewed microscopically, after which the stained area was calculated using an image-analysis system (BIOREVO BZ-9000 and BZ-H1C, Keyence Japan, Osaka, Japan).

Flow Cytometry. Isolated hepatic inflammatory cells were incubated in PBS supplemented with 2% bovine serum albumin (Sigma-Aldrich, St. Louis, MO) for 10 minutes at 4°C. The cells were incubated with fluorescein isothiocyanate (FITC)-conjugated anti-CD4 (eBioscience) and phycoerythrin (PE)-conjugated anti-CD8 antibodies (eBioscience) for 30 minutes at 4°C before examination using a FACSCalibur cytometer (BD Biosciences). Similarly, ADSCs were incubated with PE-conjugated CD90 (Beckman Coulter, Fullerton, CA), or PE-conjugated CD105 (Miltenyi Biotec). The data were analyzed using the FlowJo software (Tree Star, Ashland, OR).

DNA Microarray Analysis. Isolated RNAs were amplified and labeled with Cy3 using a QuickAmp Labeling Kit (Agilent Technologies, Santa Clara, CA) in accordance with the manufacturer's protocol. cRNA (825 ng) was hybridized onto a Whole Mouse Genome 4 × 44K Array (Agilent Technologies). The hybridized microarray slide was scanned using a DNA microarray scanner (model G2505B; Agilent Technologies).

Gene expression analysis was carried out using GeneSpring analysis software (Agilent Technologies). Each measurement was divided by the 75th percentile of all measurements in that sample to normalize per chip. Hierarchical clustering and principal component analysis of gene expression was performed. Welch's t test with Benjamini and Hochberg's false-discovery rate were used to identify differentially expressed genes in the groups of interest. Analysis of biological processes was performed using the MetaCore software suite (GeneGo, San Diego, CA). BRB array tools (http://linus.nci.nih.gov/BRB-ArrayTools.html) were also used for unsupervised clustering or one-way clustering analysis. Microarray data were deposited in the NBCI Gene Expression Omnibus (GSE ID: GSE40395).

Statistical Analysis. GraphPad Prism (v. 5.0; GraphPad Software, La Jolla, CA) was used to perform a Mann-Whitney U test to compare data between two groups, and differences were considered statistically significant at $P < 0.05$.

All other materials and methods are described in the Supporting Information.

Results

Characteristics of the NASH Mouse Model. The pathological and clinical features of cirrhosis in patients are not well replicated by the majority of chemically induced murine cirrhotic liver models. We have established steatohepatitis as a cirrhotic liver mouse model by feeding mice an Ath+HF diet.[13] When mice were fed this diet for 34 weeks, hepatocytes developed steatosis, Mallory-Denk bodies, and ballooning (Fig. 1A,B), which are identical to typical pathological features of clinical NASH.[15] Albumin expression in parenchymal cells of the cirrhotic liver significantly decreased in mice fed the Ath+HF diet for 24 weeks (Fig. 1C), while alpha-fetoprotein (AFP) expression was not affected (Fig. 1D). Fibrosis developed and reached maximal levels after 34 weeks of feeding the Ath+HF diet (Fig. 1E,F). Immunohistochemical staining for immunomodulatory cells showed an increased number of Gr-1$^+$ cells in the liver of the steatohepatitis mice fed the Ath+HF diet for 12, 34, and 70 weeks (Fig. 2A,B). The number of CD11b$^+$ cells in the liver also increased and reached maximal levels after 34 weeks of feeding the Ath+HF diet (Fig. 2C,D). Thus, the murine cirrhosis model established by an Ath+HF diet mimics the features of clinical NASH.

Effect of ADSCs Treatment on Liver Albumin Expression and Fibrosis. Adipose tissue contains MSCs, which have the potential to differentiate into several types of cell lineages[10,14] and to act as immunomodulators.[11] In this study, we isolated stromal cells from inguinal adipose tissue of GFP-expressing transgenic (GFP-Tg) mice as ADSCs and expanded them in culture. The majority of these cells expressed CD90 and CD44, known surface markers of mesenchymal cells (Supporting Fig. 1A). A proportion of the expanded ADSCs also expressed CD105 (Supporting Fig. 1B), which has been recognized as a representative surface marker of MSCs.[11]

We evaluated whether ADSCs could provide a therapeutically beneficial treatment for liver cirrhosis in steatohepatitis mice. We injected 1×10^5 GFP-ADSCs by way of the spleen/portal vein in mice fed the Ath+HF diet for 32 weeks. We observed that the GFP-ADSCs resided in all lobes of the liver at 3, 7, and 14 days after injection (Fig. 3A,B). Importantly, immunohistochemical staining showed that GFP$^+$ cells in the cirrhotic liver expressed higher levels of albumin than did the surrounding parenchymal cells (Fig. 3C).

We also injected 1×10^5 or 2×10^4 GFP-ADSCs twice every 2 weeks by way of the splenic/portal vein

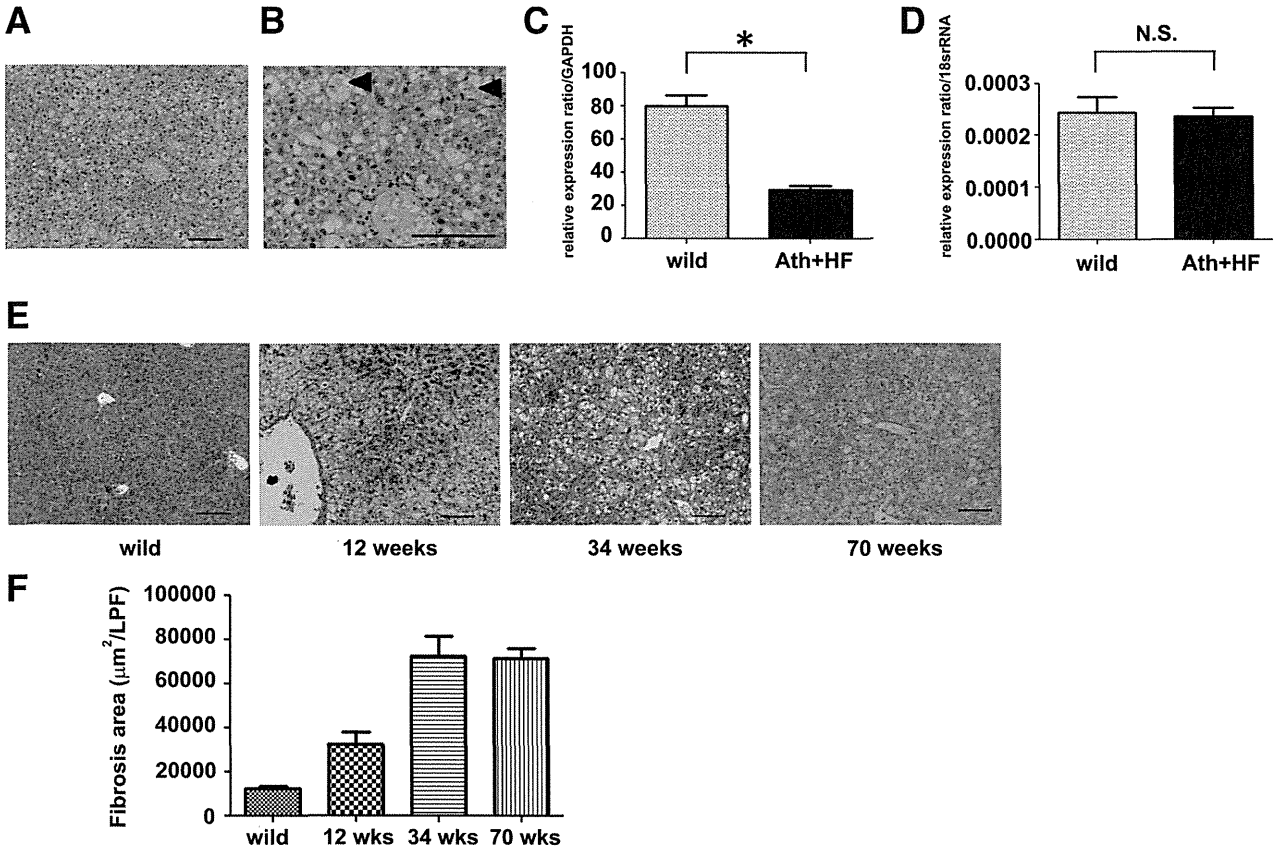

Fig. 1. Characteristics of the steatohepatitis murine model. Eight-week-old C57Bl/6 female mice were fed an Ath+HF diet. Liver tissue was obtained after 34 weeks, sectioned, and histologically examined with hematoxylin and eosin staining in (A,B) mice fed an Ath+HF diet for 34 weeks. Arrowheads indicate a Mallory-Denk body in a hepatocyte with ballooning. Parenchymal cells were isolated from 32-week-old C57Bl/6 wild-type female mice or Ath+HF mice that started the diet at 8 weeks old and continued for 24 weeks. Expression of (C) albumin and (D) AFP was assessed by reverse-transcription polymerase chain reaction (RT-PCR), n = 4, $*P < 0.05$. (E) Fibrosis was histologically examined with Azan staining in liver tissue of mice fed the Ath+HF diet for 12, 34, and 70 weeks. (F) Fibrosis areas of mice at 12, 34, and 70 weeks per ×100 low-power field were calculated for five visual fields. Bars: standard error. Scale bars = 100 μm.

in mice fed an Ath+HF diet for 32 or 36 weeks, respectively. Two weeks after the last injection the mice were euthanized and the therapeutic effects were assessed. The expression of albumin (Fig. 4A) was restored in hepatic parenchymal cells of cirrhotic mice at 2 weeks after the last injection, suggesting that ADSC treatment restored parenchymal cell function. The expression of AFP was also increased by ADSC treatment (Fig. 4B), implying enhanced regeneration of hepatic parenchymal cells. Similar effects were observed with a reduced number of (2×10^4) GFP-ADSCs (Supporting Fig. 2A,B).

We also assessed the effect of ADSC injection on fibrosis in cirrhotic mice. Liver tissue stained with Azan and anticollagen type IV antibody showed that ADSC administration reduced fibrosis compared to control animals (Fig. 5A,B; Supporting Fig. S3A,B). We also evaluated immunohistochemical staining of α-SMA, a marker of stellate cells, which are largely responsible for developing fibrosis. These results demonstrated that the number of α-SMA$^+$ cells was reduced by ADSC treatment (Fig. 5C-E), suggesting that ADSCs suppress the activity of stellate cells and ameliorate liver fibrosis.

Gene Expression Profiling of Cirrhotic Livers Following ADSC Treatment. We examined the gene expression profile of the livers in the NASH mouse model of cirrhosis by DNA microarray to determine whether administration of ADSCs was therapeutically beneficial. We identified expression of 1,249 gene probes that were significantly affected by ADSC injection. Clustering analysis of gene expression using these gene probes distinguished between ADSCs-treated mice and PBS-treated mice (Fig. 6A). Among 1,249 genes, 797 were up-regulated and 452 were down-regulated by ADSC treatment. Regarding matrix metalloproteinase (MMP), expressions of MMP-8 and MMP-9 were enhanced in the liver of NASH mice treated with PBS compared to the wild type; this enhancement was removed by ADSC treatment

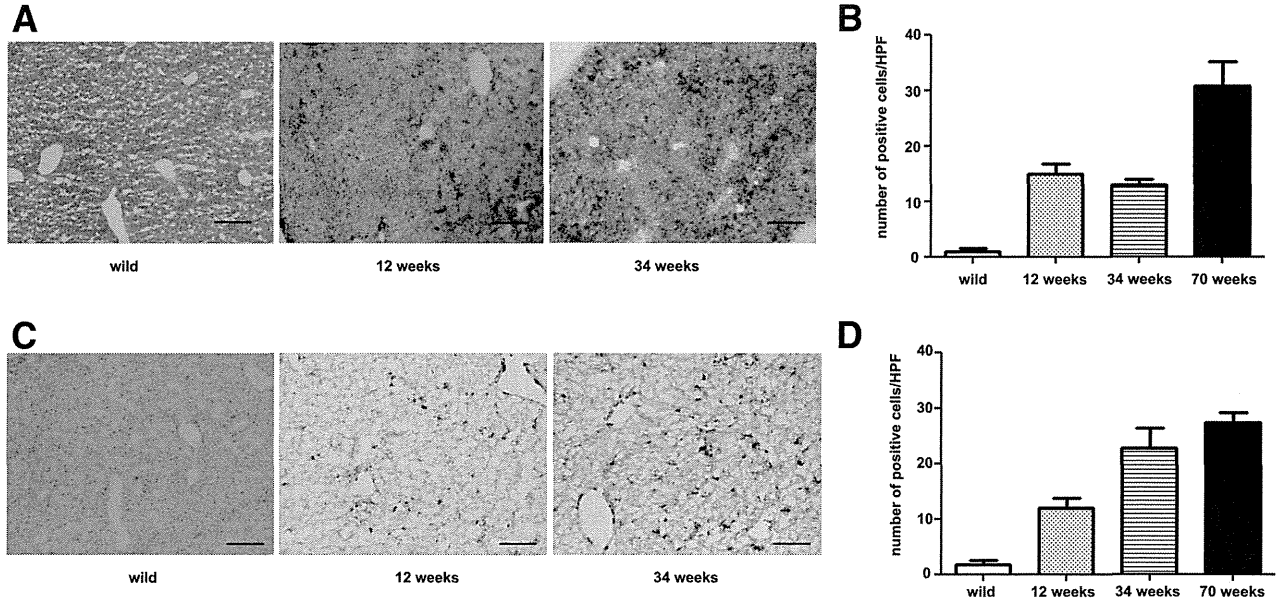

Fig. 2. Immunohistochemical staining of a steatohepatitis liver. Eight-week-old female C57Bl/6 female mice were fed an Ath+HF diet. Liver tissue was obtained from these mice or from wild-type animals after 12, 34, and 70 weeks. Immunohistochemical staining was performed for (A) Gr-1$^+$ or (C) CD11b$^+$ cells and the number of positive cells in a high-power field was counted for five visual fields for (B) Gr-1 or (D) CD11b at each timepoint.

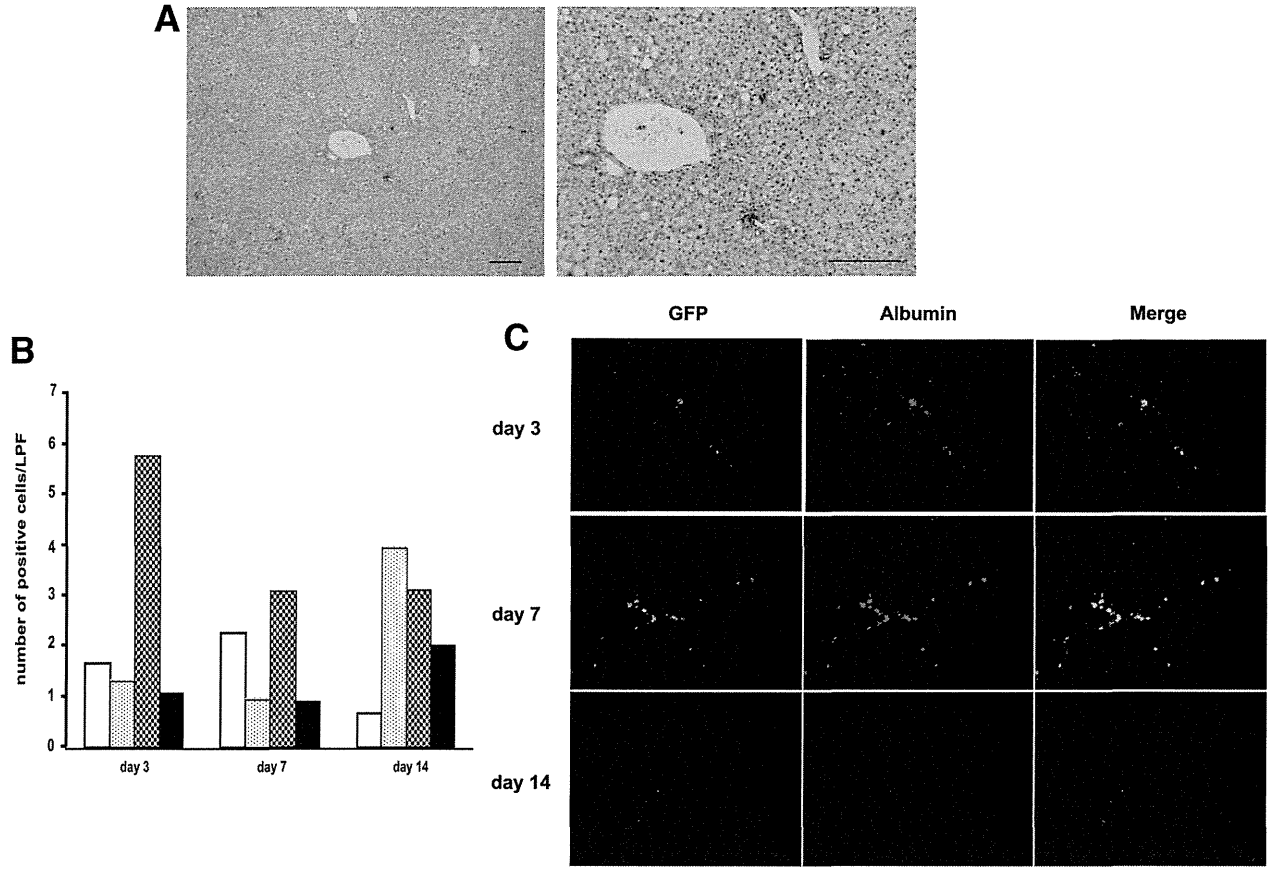

Fig. 3. Distribution of ADSCs and albumin expression in the livers of steatohepatitis mice. ADSCs from GFP-Tg mice (1×10^5) were injected into the splenic subcapsule of cirrhotic C57Bl/6 mice fed the Ath+HF diet for 32 weeks. After 3, 7, and 14 days, liver tissue was obtained and examined by immunohistochemical staining for (A) GFP; Scale bars = 100 μm. (B) GFP$^+$ cells in the liver were counted per ×100 low-power field and five visual fields were calculated. White bar, caudate lobe; dotted bar, left lobe; hatched bar, middle lobe; black bar, right lobe. (C) Immunohistochemical staining for GFP or albumin antibody. Magnification, ×100.

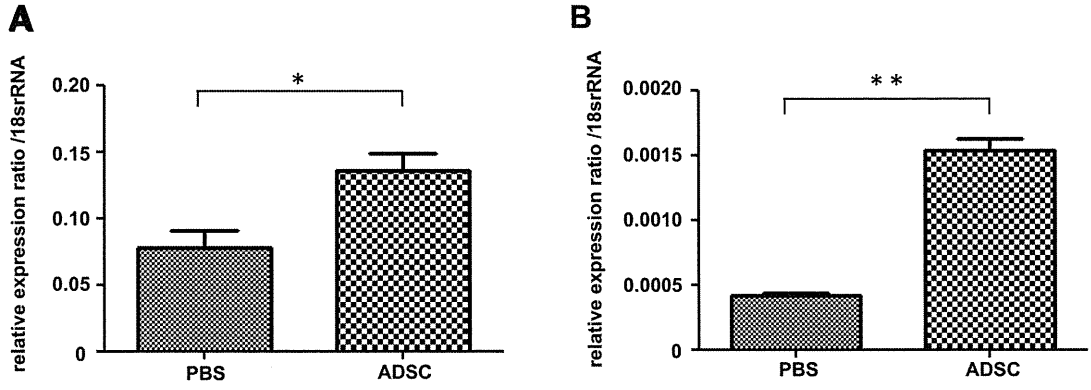

Fig. 4. Albumin and AFP expression in hepatic parenchymal cells. ADSCs from GFP-Tg mice (1×10^5) were injected twice every 2 weeks into the splenic subcapsule of cirrhotic C57Bl/6 mice fed an Ath+HF diet for 32 weeks. Control mice received PBS injections. Two weeks after the last injection, liver tissue was obtained and parenchymal cells were isolated for real-time PCR. Expressions of (A) albumin and (B) AFP were normalized relative to that of 18S ribosomal RNA (rRNA); $*P < 0.05$, $**P < 0.01$.

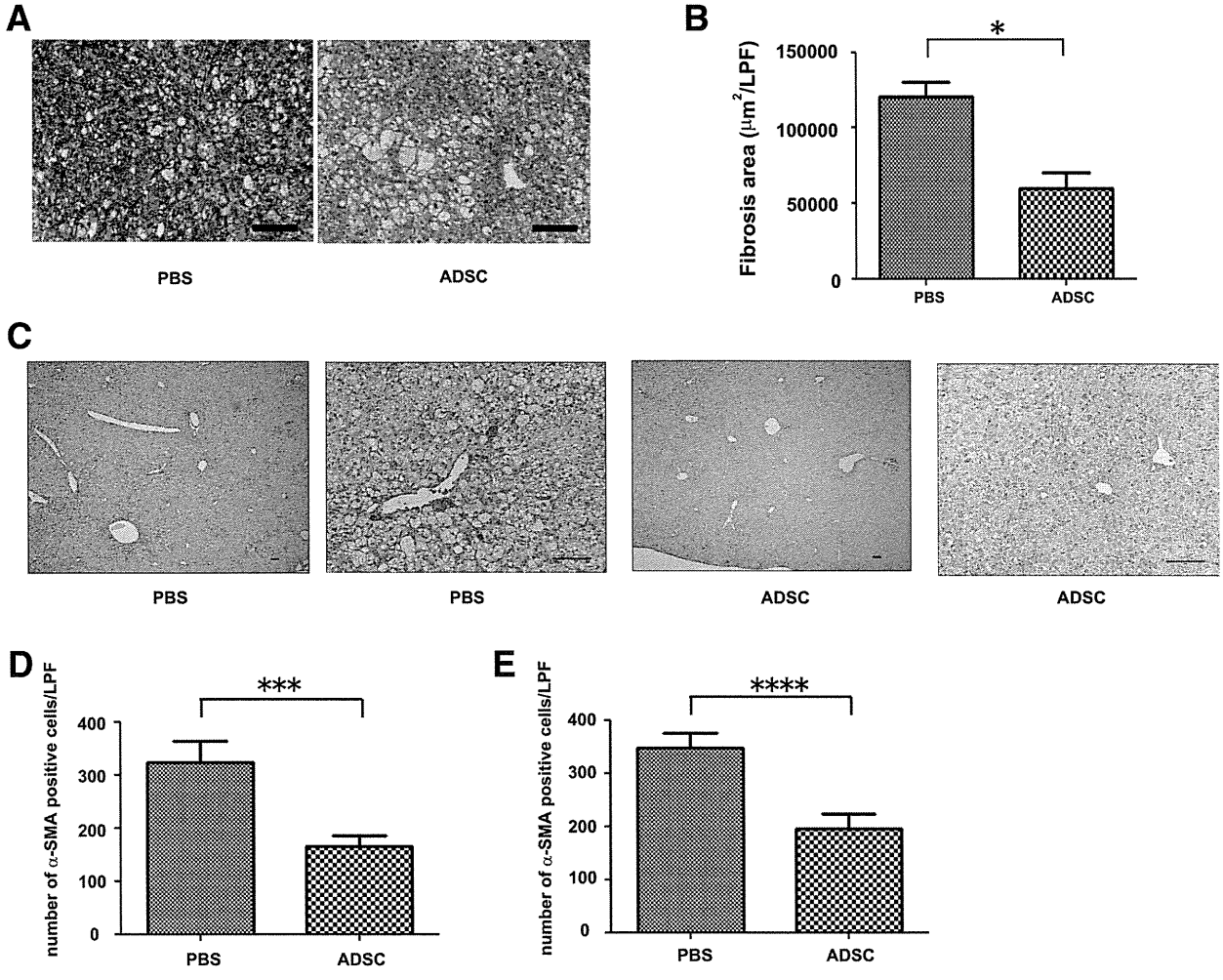

Fig. 5. Effect of ADSCs on liver fibrosis. ADSCs from GFP-Tg mice (1×10^5) were injected twice every 2 weeks into the splenic subcapsule of cirrhotic C57Bl/6 mice fed the Ath+HF diet for 32 weeks. Control mice received PBS injections. (A) Two weeks after the last injection, liver tissue was obtained, sectioned, and histologically examined with hematoxylin and eosin staining. (B) Fibrosis was examined by Azan staining and fibrotic area was quantified by image-analysis. (C) Immunohistochemical staining of liver sections for α-SMA. Scale bars = 100 μm. (D,E) The number of α-SMA+ cells in liver tissues obtained 1 (D) or 2 weeks (E) after the last ADSC injection determined by microscopy of five low-power fields (×100); $***P < 0.005$, $****P = 0.0001$.

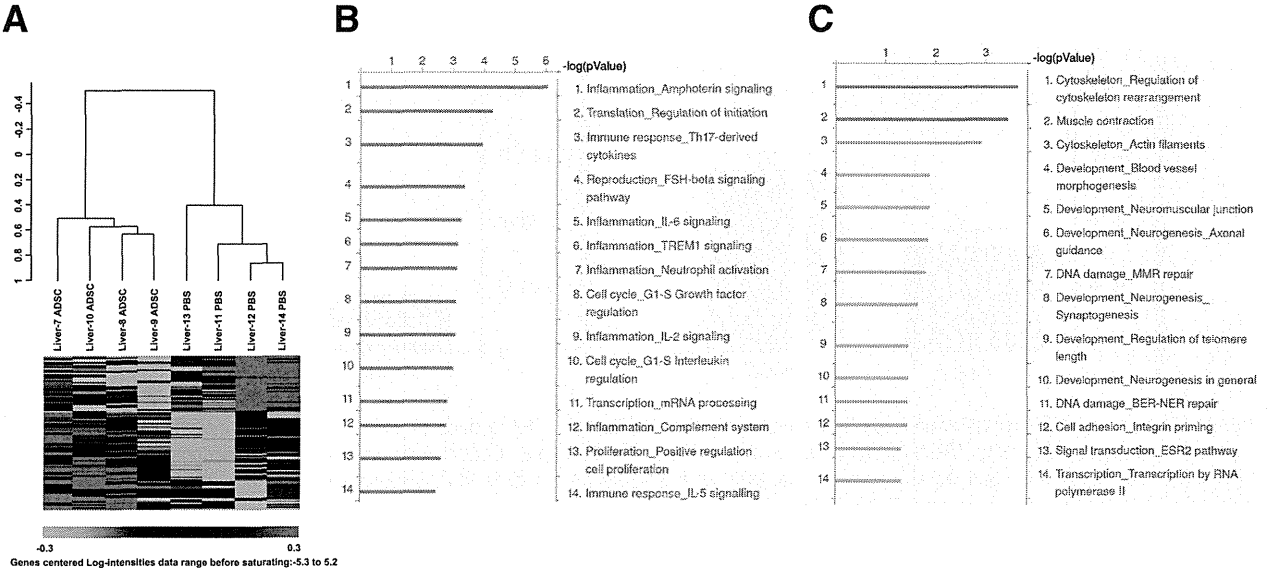

Fig. 6. Hepatic gene expression analysis. ADSCs from GFP-Tg mice (1×10^5) were injected twice every 2 weeks into the splenic subcapsule of cirrhotic C57Bl/6 mice fed an Ath+HF diet for 40 weeks. Control mice received PBS injections. Two weeks later, liver tissue was subjected to RNA isolation and gene expression using DNA microarrays. (A) Unsupervised clustering analysis was performed using probes for 1,249 genes whose expression differed significantly between the PBS and ADSC groups. (B) The biological processes of 452 genes whose expression was down-regulated in the ADSCs group compared to the PBS group were analyzed. (C) The biological processes of 797 genes whose expression was up-regulated in the ADSCs group compared to the PBS group were analyzed.

(Supporting Fig. S4). Biological process analysis indicated that the down-regulated genes were primarily related to inflammation and the immune response (Fig. 6B), and the up-regulated genes were related to tissue construction and development (Fig. 6C). Thus, gene expression analysis of liver tissue demonstrated that ADSCs treatment caused anti-inflammatory effects, as well as regeneration/repair effects, in the livers of a NASH mouse model of cirrhosis.

Anti-inflammatory Effects of ADSC Treatment. The fundamental underlying pathophysiology of steatohepatitis-induced cirrhosis is persistent hepatic inflammation caused by steatosis in hepatocytes.[16] We examined how ADSCs affected persistent inflammation of the liver in NASH mice at 2 weeks after the last injection of ADSCs. Immunohistochemical staining showed that the number of $CD11b^+$ cells accumulating in the livers of cirrhotic mice decreased with ADSC treatment compared to those of PBS-treated mice (Fig. 7A). The number of $Gr\text{-}1^+$ cells in cirrhotic liver also decreased with ADSC treatment (Fig. 7A), suggesting that ADSCs affect granulocytes and antigen-presenting cell lineage.

We further examined whether ADSC treatment affected the lymphocyte lineage of T cells, since they also play an important role in immune regulation of steatohepatitis.[17] We isolated lymphocytes from the livers of mice treated with ADSCs and examined the $CD4^+$ and $CD8^+$ T cells using flow cytometry. $CD8^+$ T cells were found predominantly in cirrhotic mice treated with PBS (Fig. 7B,C). However, when the mice were treated with ADSCs the number of $CD4^+$ T cells increased and was comparable to that of $CD8^+$ T cells, indicating that ADSC treatment affected T-cell subpopulations.

Gene Expression Profiling of Hepatic Inflammatory Cells Following ADSC Treatment. We further examined how injected ADSCs affected hepatic inflammatory cell gene expression by using DNA microarrays. By filtering the results from 5,065 gene probes, completely discernible clusters of gene expression were formed between ADSC- and PBS-treated animals (Fig. 8A). We identified the expression of 873 genes that were significantly up-regulated at least 2-fold with ADSC injection and 658 genes that were down-regulated. Most of the chemokines and cytokines whose expression was significantly affected by ADSCs were down-regulated (Supporting Table S1). Using the publicly available gene expression database for hematopoietic cells (GSE27787) and various types of helper T cells (GSE14308), we examined features of these affected genes in the context of immunomodulatory cells. Among the hematopoietic cells, genes with available symbol annotation were predominately $Gr\text{-}1^+$ and $CD11b^+$ cells from granulocyte and macrophage lineages (Fig. 8B). Among helper T-cell populations,

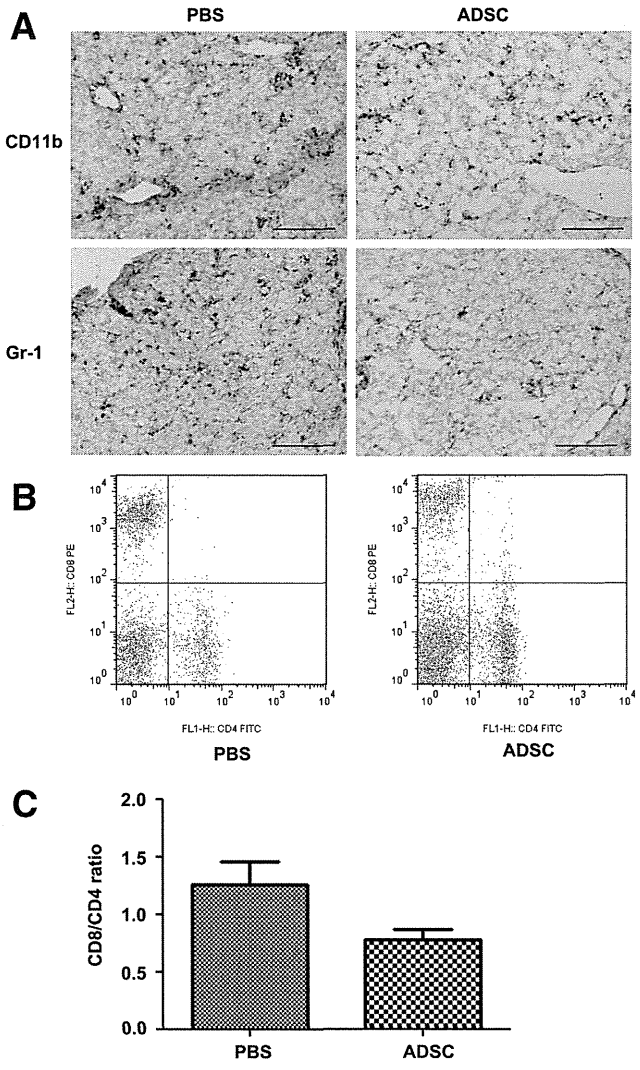

Fig. 7. Effect of ADSCs on inflammatory cells in the cirrhotic liver. ADSCs from GFP-Tg mice (1×10^5) were injected twice every 2 weeks into the splenic subcapsule of cirrhotic C57Bl/6 mice fed the Ath+HF diet for 32 weeks. Control mice received PBS injections. Two weeks later, liver tissue was obtained and immunohistochemical staining of (A) $CD11b^+$ and (B) $Gr\text{-}1^+$ cells was performed. Inflammatory cells in the liver were also isolated and stained with FITC-labeled anti-CD4 and PE-labeled CD8 antibodies. (C) The ratio of $CD8^+$ cells to $CD4^+$ cells was calculated. N = 4 ± standard error.

annotated genes included activated Th1, Th2, and Th17 cell types (Fig. 8C). We also isolated $CD4^+$T cells from hepatic inflammatory cells obtained from NASH mice fed an Ath+HF diet for 12 weeks, then treated with ADSC. Expressions of the Th1, Th2, and Th17 cytokines, interferon-γ, interleukin (IL)−4, IL-10, and IL-17, the Th17-related cytokine transforming growth factor beta (TGF-β), and Foxp3, a representative transcription factor of regulatory T cells, were down-regulated by ADSC treatment (Supporting Fig. S5).

These results suggest that ADSC treatment suppresses inflammation in the NASH mouse model primarily by down-regulating granulocytes, antigen-presenting cells, and activated helper T cells.

Discussion

This study investigated the therapeutic effect of ADSCs in a NASH murine model of cirrhosis. This model is relevant to clinical NASH, with similar pathological features established by an atherogenic high-fat diet, including the appearance of steatosis, ballooning, and Mallory-Denk bodies in hepatocytes, infiltration of inflammatory cells, and pericellular fibrosis. Our results demonstrate that ADSC injection is therapeutically beneficial for cirrhosis in this murine model through restoration of albumin expression in hepatic parenchymal cells, amelioration of fibrosis, and suppression of persistent hepatic inflammation.

Gene expression analysis of the liver in this cirrhotic mouse model revealed that ADSC injection affects biological processes relating to anti-inflammatory and regeneration/repair pathways. The anti-inflammatory effects are mediated by ADSC targeting of $Gr\text{-}1^+$, $CD11b^+$, and helper T-cell lineages. In patients with clinical NASH, the ratio of neutrophils to lymphocytes increases,[18] suggesting that granulocytes are involved in the pathogenesis of NASH. The NASH murine model used in this study produced an increased $CD8^+/CD4^+$ T-cell ratio, which is also comparable to clinical NASH patient pathology.[19] Gene expression analysis of liver tissue and hepatic inflammatory cells from NASH mice showed that Th1-, Th2-, and Th17-related genes were down-regulated by ADSC treatment. Helper T-cell activation skewed to produce Th1 cytokines is pathogenic in steatohepatitis.[20,21] In particular, Th17 is emerging as an important source of IL-17 family cytokines[22] and is involved in the hepatic inflammation in NASH.[23] Helper T cells producing Th2 cytokines such as IL-4, 5, and 13 contribute to fibrosis.[24] We conclude that activated T helper cells are responsible for the pathogenesis of steatohepatitis in the NASH murine model used in this study and that ADSCs suppress pathogenic helper T-cell activation. However, the suppression of miscellaneous effector and regulatory helper T cells by ADSCs should be further evaluated with regard to prevention of hepatocellular carcinoma, a frequent sequela to cirrhosis, since Th1 promotes antitumor immunity and Th2 down-regulates antitumor immunity.

We also observed that ADSC treatment ameliorated fibrosis and decreased the number of α-SMA^+ stellate

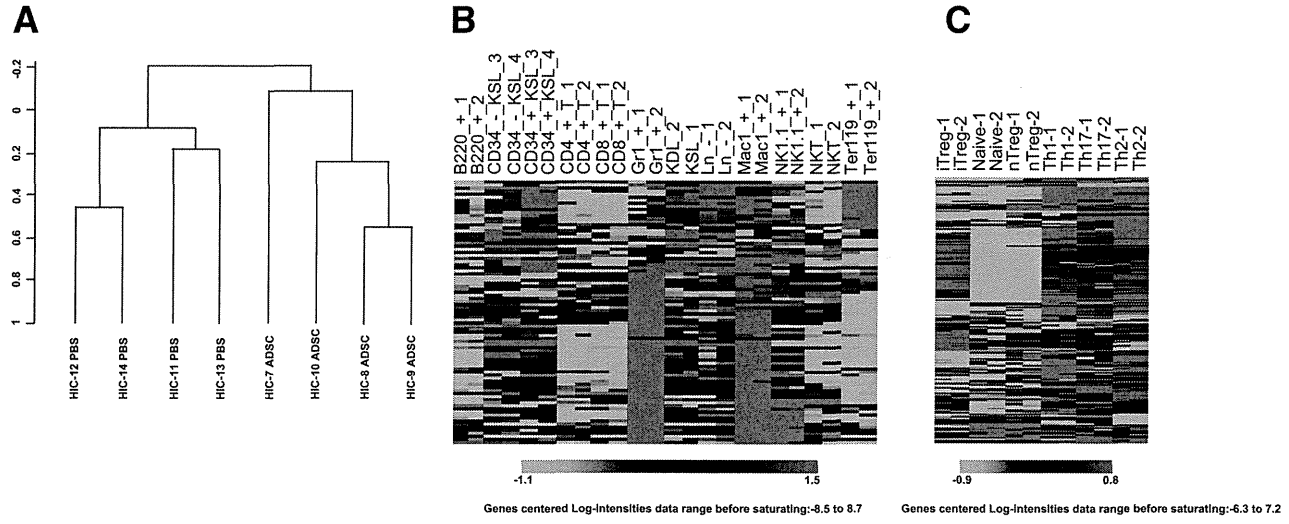

Fig. 8. Gene-expression analysis of intrahepatic inflammatory cells. ADSCs from GFP-Tg mice (1×10^5) were injected twice every 2 weeks into the splenic subcapsule of cirrhotic C57Bl/6 mice fed an Ath+HF diet for 40 weeks. Control mice received PBS injections. Inflammatory cells were isolated from the liver and gene expression examination was performed using DNA microarrays. (A) Unsupervised clustering analysis using the filtered 5,065 gene probes. HIC; hepatic inflammatory cells. (B) One-way clustering analysis using a publicly available database of hematopoietic cells (GSE27787) of 658 genes whose expression was down-regulated by ADSC treatment with available gene symbol annotations. (C) One-way clustering analysis using publicly available database of different helper T subsets (GSE14308) of 658 genes whose expression was down-regulated by ADSCs treatment with available gene symbol annotations.

cells in cirrhotic liver. When inflammation persists in the liver, fibrosis progresses due to these activated stellate cells, which are almost identical to myofibroblasts and produce extracellular matrix. Stellate cells are activated by miscellaneous factors including TGF-β and platelet-derived growth factor,[25] produced mostly from Kupffer cells. Helper T cells expressing Th2 cytokines are also involved in the development of fibrosis. Gene expression analysis of the cirrhotic livers indicated that ADSC treatment suppressed Th2-type helper T cells. Although details of how these molecules mediate fibrosis development have yet to be examined in the current NASH murine model, the antifibrotic effect of ADSCs is achieved in part by suppressing Th2-type helper T cells. We found that MMP-8 and MMP-9 enhancement in the NASH-cirrhotic liver was ameliorated by ADSC treatment. MMP-9 expression is related to the inflammation typical of steatohepatitis[26] and can ameliorate the hepatic fibrosis induced by carbon tetrachloride.[27] Further studies are needed to clarify the role of MMPs in the pathogenesis of cirrhosis as well as to explore novel therapies for this condition.

Pluripotent MSCs differentiate into several cell lineages and are a promising avenue for regenerative therapy of various impaired organs, including the liver. Although ADSCs were observed in cirrhotic livers at up to 2 weeks after injection and expressed albumin, the numbers of resident cells were not sufficient to supplement hepatic function. Therefore, pluripotency, as well as the anti-inflammatory and antifibrotic effects of ADSCs, are important for their regenerative/repair effects in liver cirrhosis. Rather than studying the effects of ADSCs on early-stage steatohepatitis, we treated mice with endstage cirrhosis with ADSCs to observe their therapeutic effects. Our results demonstrated that ADSCs can effectively resolve chronic fibrosis and decrease inflammation, thereby restoring hepatic function in endstage cirrhotic mice, implying the usefulness of this therapy as an alternative to liver transplantation.

In conclusion, ADSCs proved therapeutically beneficial and clinically relevant in regenerative therapy of a murine steatohepatitis-cirrhosis model. Clinical application of ADSCs in the treatment of cirrhosis is expected to provide a novel alternative regenerative/repair therapy for patients with cirrhosis.

References

1. D'Amico G, Garcia-Tsao G, Pagliaro L. Natural history and prognostic indicators of survival in cirrhosis: a systematic review of 118 studies. J Hepatol 2006;44:217-231.
2. Llovet JM, Burroughs A, Bruix J. Hepatocellular carcinoma. Lancet 2003;362:1907-1917.
3. Fattovich G, Stroffolini T, Zagni I, Donato F. Hepatocellular carcinoma in cirrhosis: incidence and risk factors. Gastroenterology 2004;127:S35-50.
4. Kamath PS, Kim WR. The model for end-stage liver disease (MELD). HEPATOLOGY 2007;45:797-805.
5. Stravitz RT, Carl DE, Biskobing DM. Medical management of the liver transplant recipient. Clin Liver Dis 2011;15:821-843.

6. Forner A, Llovet JM, Bruix J. Hepatocellular carcinoma. Lancet 2012;379:1245-1255.
7. Chamberlain G, Fox J, Ashton B, Middleton J. Concise review: mesenchymal stem cells: their phenotype, differentiation capacity, immunological features, and potential for homing. Stem Cells 2007;25:2739-2749.
8. Franco Lambert AP, Fraga Zandonai A, Bonatto D, Cantarelli Machado D, Pegas Henriques JA. Differentiation of human adipose-derived adult stem cells into neuronal tissue: does it work? Differentiation 2009;77:221-228.
9. Banas A, Teratani T, Yamamoto Y, Tokuhara M, Takeshita F, Osaki M, et al. Rapid hepatic fate specification of adipose-derived stem cells and their therapeutic potential for liver failure. J Gastroenterol Hepatol 2009;24:70-77.
10. Banas A, Teratani T, Yamamoto Y, Tokuhara M, Takeshita F, Quinn G, et al. Adipose tissue-derived mesenchymal stem cells as a source of human hepatocytes. HEPATOLOGY 2007;46:219-228.
11. Uccelli A, Moretta L, Pistoia V. Immunoregulatory function of mesenchymal stem cells. Eur J Immunol 2006;36:2566-2573.
12. Zuk PA, Zhu M, Ashjian P, De Ugarte DA, Huang JI, Mizuno H, et al. Human adipose tissue is a source of multipotent stem cells. Mol Biol Cell 2002;13:4279-4295.
13. Matsuzawa N, Takamura T, Kurita S, Misu H, Ota T, Ando H, et al. Lipid-induced oxidative stress causes steatohepatitis in mice fed an atherogenic diet. HEPATOLOGY 2007;46:1392-1403.
14. Furuichi K, Shintani H, Sakai Y, Ochiya T, Matsushima K, Kaneko S, et al. Effects of adipose-derived mesenchymal cells on ischemia-reperfusion injury in kidney. Clin Exp Nephrol 2012;16:579-589.
15. Brunt EM. Nonalcoholic steatohepatitis: definition and pathology. Semin Liver Dis 2001;21:3-16.
16. Cohen JC, Horton JD, Hobbs HH. Human fatty liver disease: old questions and new insights. Science 2011;332:1519-1523.
17. Inzaugarat ME, Ferreyra Solari NE, Billordo LA, Abecasis R, Gadano AC, Chernavsky AC. Altered phenotype and functionality of circulating immune cells characterize adult patients with nonalcoholic steatohepatitis. J Clin Immunol 2011;31:1120-1130.
18. Alkhouri N, Morris-Stiff G, Campbell C, Lopez R, Tamimi TA, Yerian L, et al. Neutrophil to lymphocyte ratio: a new marker for predicting steatohepatitis and fibrosis in patients with nonalcoholic fatty liver disease. Liver Int 2012;32:297-302.
19. Susca M, Grassi A, Zauli D, Volta U, Lenzi M, Marchesini G, et al. Liver inflammatory cells, apoptosis, regeneration and stellate cell activation in non-alcoholic steatohepatitis. Dig Liver Dis 2001;33:768-777.
20. Olleros ML, Martin ML, Vesin D, Fotio AL, Santiago-Raber ML, Rubbia-Brandt L, et al. Fat diet and alcohol-induced steatohepatitis after LPS challenge in mice: role of bioactive TNF and Th1 type cytokines. Cytokine 2008;44:118-125.
21. Ferreyra Solari NE, Inzaugarat ME, Baz P, De Matteo E, Lezama C, Galoppo M, et al. The role of innate cells is coupled to a Th1-polarized immune response in pediatric nonalcoholic steatohepatitis. J Clin Immunol 2012;32:611-621.
22. Ouyang W, Kolls JK, Zheng Y. The biological functions of T helper 17 cell effector cytokines in inflammation. Immunity 2008;28:454-467.
23. Tang Y, Bian Z, Zhao L, Liu Y, Liang S, Wang Q, et al. Interleukin-17 exacerbates hepatic steatosis and inflammation in non-alcoholic fatty liver disease. Clin Exp Immunol 2011;166:281-290.
24. Wynn TA. Fibrotic disease and the T(H)1/T(H)2 paradigm. Nat Rev Immunol 2004;4:583-594.
25. Wu J, Zern MA. Hepatic stellate cells: a target for the treatment of liver fibrosis. J Gastroenterol 2000;35:665-672.
26. Wanninger J, Walter R, Bauer S, Eisinger K, Schaffler A, Dorn C, et al. MMP-9 activity is increased by adiponectin in primary human hepatocytes but even negatively correlates with serum adiponectin in a rodent model of non-alcoholic steatohepatitis. Exp Mol Pathol 2011;91:603-607.
27. Higashiyama R, Inagaki Y, Hong YY, Kushida M, Nakao S, Niioka M, et al. Bone marrow-derived cells express matrix metalloproteinases and contribute to regression of liver fibrosis in mice. HEPATOLOGY 2007;45:213-222.

HEPATOLOGY
Official Journal of the American Association for the Study of Liver Diseases

Discrete Nature of EpCAM$^+$ and CD90$^+$ Cancer Stem Cells in Human Hepatocellular Carcinoma

Taro Yamashita,[1] Masao Honda,[1] Yasunari Nakamoto,[1] Masayo Baba,[1] Kouki Nio,[1] Yasumasa Hara,[1] Sha Sha Zeng,[1] Takehiro Hayashi,[1] Mitsumasa Kondo,[1] Hajime Takatori,[1] Tatsuya Yamashita,[1] Eishiro Mizukoshi,[1] Hiroko Ikeda,[1] Yoh Zen,[1] Hiroyuki Takamura,[1] Xin Wei Wang,[2] and Shuichi Kaneko[1]

Recent evidence suggests that hepatocellular carcinoma (HCC) is organized by a subset of cells with stem cell features (cancer stem cells; CSCs). CSCs are considered a pivotal target for the eradication of cancer, and liver CSCs have been identified by the use of various stem cell markers. However, little information is known about the expression patterns and characteristics of marker-positive CSCs, hampering the development of personalized CSC-targeted therapy. Here, we show that CSC markers EpCAM and CD90 are independently expressed in liver cancer. In primary HCC, EpCAM$^+$ and CD90$^+$ cells resided distinctively, and gene-expression analysis of sorted cells suggested that EpCAM$^+$ cells had features of epithelial cells, whereas CD90$^+$ cells had those of vascular endothelial cells. Clinicopathological analysis indicated that the presence of EpCAM$^+$ cells was associated with poorly differentiated morphology and high serum alpha-fetoprotein (AFP), whereas the presence of CD90$^+$ cells was associated with a high incidence of distant organ metastasis. Serial xenotransplantation of EpCAM$^+$/CD90$^+$ cells from primary HCCs in immunedeficient mice revealed rapid growth of EpCAM$^+$ cells in the subcutaneous lesion and a highly metastatic capacity of CD90$^+$ cells in the lung. In cell lines, CD90$^+$ cells showed abundant expression of c-Kit and *in vitro* chemosensitivity to imatinib mesylate. Furthermore, CD90$^+$ cells enhanced the motility of EpCAM$^+$ cells when cocultured *in vitro* through the activation of transforming growth factor beta (TGF-β) signaling, whereas imatinib mesylate suppressed *TGFB1* expression in CD90$^+$ cells as well as CD90$^+$ cell-induced motility of EpCAM$^+$ cells. *Conclusion*: Our data suggest the discrete nature and potential interaction of EpCAM$^+$ and CD90$^+$ CSCs with specific gene-expression patterns and chemosensitivity to molecular targeted therapy. The presence of distinct CSCs may determine the clinical outcome of HCC. (HEPATOLOGY 2013;57:1484-1497)

The cancer stem cell (CSC) hypothesis, which suggests that a subset of cells bearing stem-cell–like features is indispensable for tumor development, has recently been put forward subsequent to advances in molecular and stem cell biology. Liver cancer, including hepatocellular carcinoma (HCC), is a leading cause of cancer death worldwide.[1] Recent studies have shown the existence of CSCs in liver cancer cell lines and primary HCC specimens using various stem cell markers.[2-7] Independently, we have identified novel HCC subtypes defined by the hepatic stem/progenitor cell markers,

Abbreviations: 5-FU, fluorouracil; Abs, antibodies; AFP, alpha-fetoprotein; CK-19, cytokeratin-19; CSC, cancer stem cell; DNs, dysplastic nodules; EMT, epithelial mesenchymal transition; EpCAM; epithelial cell adhesion molecule; FACS, fluorescent-activated cell sorting; HBV, hepatitis B virus; HCC, hepatocellular carcinoma; HCV, hepatitis C virus; HSCs, hepatic stem cells; IF, immunofluorescence; IHC, immunohistochemistry; IR, immunoreactivity; MDS, multidimensional scaling; NBNC, non-B, non-C hepatitis; NOD/SCID, nonobese diabetic, severe combined immunodeficient; NT, nontumor; OV-1, ovalbumin 1; qPCR, quantitative real-time polymerase chain reaction; SC, subcutaneous; Smad3, Mothers against decapentaplegic homolog 3; TECs, tumor epithelial cells; TGF-β, transforming growth factor beta; T/N, tumor/nontumor; VECs, vascular endothelial cells; VM, vasculogenic mimicry; VEGFR, vascular endothelial growth factor receptor.

From the [1]Liver Center, Kanazawa University Hospital, Kanazawa, Ishikawa, Japan; and [2]Laboratory of Human Carcinogenesis, Center for Cancer Research, National Cancer Institute, Bethesda, MD.

Received July 9, 2012; revised October 22, 2012; accepted November 6, 2012.

This study was supported by a Grant-in-Aid from the Ministry of Education, Culture, Sports, Science, and Technology of Japan (23590967), a grant from the Japanese Society of Gastroenterology, a grant from the Ministry of Health, Labor, and Welfare, and a grant from the National Cancer Center Research and Development Fund (23-B-5) of Japan. X.W.W. is supported by the Intramural Research Program of the Center for Cancer Research, U.S. National Cancer Institute.

epithelial cell adhesion molecule (EpCAM) and alpha-fetoprotein (AFP), which correlate with distinct gene-expression signatures and prognosis.[8,9] EpCAM$^+$ HCC cells isolated from primary HCC and cell lines show CSC features, including tumorigenicity, invasiveness, and resistance to fluorouracil (5-FU).[10] Similarly, other groups have shown that CD133$^+$, CD90$^+$, and CD13$^+$ HCC cells are also CSCs, and that EpCAM, CD90, and CD133 are the only markers confirmed to enrich CSCs from primary HCCs thus far.[3-5,10]

Although EpCAM$^+$, CD90$^+$, and CD133$^+$ cells show CSC features, such as high tumorigenicity, an invasive nature, and resistance to chemo- and radiation therapy, it remains unclear whether these cells represent an identical HCC population and whether they share similar or distinct characteristics. In this study, we used fluorescent-activated cell sorting (FACS), microarray, and immunohistochemistry (IHC) techniques to investigate the expression patterns of the representative liver CSC markers CD133, CD90, and EpCAM in a total of 340 HCC cases and 7 cases of mesenchymal liver tumors. We further explored gene- and protein-expression patterns as well as tumorigenic capacity of sorted cells isolated from 15 primary HCCs and 7 liver cancer cell lines in an attempt to identify the molecular portraits of each cell type.

Materials and Methods

Clinical Specimens. HCC samples were obtained with informed consent from patients who had undergone radical resection at the Liver Center in Kanazawa University Hospital (Kanazawa, Japan), and tissue acquisition procedures were approved by the ethics committee of Kanazawa University. A total of 102 formalin-fixed and paraffin-embedded HCC samples, obtained from 2001 to 2007, were used for IHC analyses. Fifteen fresh HCC samples were obtained between 2008 and 2012 from surgically resected specimens and an autopsy specimen and were used immediately to prepare single-cell suspensions and xenotransplantation (Table 1). Seven hepatic stromal tumors (three cavernous hemangioma, two hemangioendothelioma, and two angiomyolipoma) were formalin fixed and paraffin embedded and used for IHC analyses.

Table 1. Clinicopathological Characteristics of HCC Cases Used for Xenotransplantation

ID	Age/ Sex	Etiology	Tumor Size (cm)	Histological Grade	AFP (ng/mL)	DCP (IU/mL)
P1	77/M	Alcohol	12.0	Moderate	198	322
P2	61/F	NBNC	11.0	Moderate	12	3,291
P3	66/M	NBNC	2.2	Moderate	13	45
P4	65/M	HCV	4.2	Poor	13,700	25,977
P5	52/M	HBV	6.0	Moderate	29,830	1,177
P6	60/M	HCV	2.7	Poor	249	185
P7	79/F	HBV	4.0	Poor	46,410	384
P8	77/F	NBNC	5.5	Moderate	17,590	562
P9	71/M	Alcohol	7.0	Poor	3,814	607
P10	51/M	HBV	2.2	Well	<10	21
P11	71/M	Alcohol	2.1	Well	<10	11
P12	60/M	HBV	10.8	Poor	323	2,359
P13	66/M	HCV	2.8	Moderate	11	29
P14	71/M	HCV	7.2	Moderate	235,700	375,080
P15	75/M	HBV	5.5	Poor	<10	97

Abbreviation: DCP, des-gamma-carboxy prothrombin.

Additional details of experimental procedures are available in the Supporting Information.

Results

EpCAM, CD133, and CD90 Expression in HCC. We first evaluated the frequencies of three representative CSC markers (EpCAM$^+$, CD90$^+$, and CD133$^+$ cells) in 12 fresh primary HCC cases surgically resected by FACS (representative data shown in Fig. 1A). Clinicopathological characteristics of primary HCC cases are shown in Table 1. We noted that frequency of EpCAM$^+$, CD90$^+$, and CD133$^+$ cells varied between individuals. Abundant CD90$^+$ (7.0%), but almost no EpCAM$^+$, cells (0.06%, comparable to the isotype control) were detected in P2, whereas few CD90$^+$ (0.6%), but abundant EpCAM$^+$, cells (17.5%) were detected in P4. Very small populations of EpCAM$^+$ (0.09%), CD90$^+$ (0.04%), and CD133$^+$ cells (0.05%) were found in P12, but they were almost nonexistent in P8, except for CD90$^+$ cells (0.08%) (Fig. 1A). We further evaluated the expression of EpCAM, CD90, and CD133 in xenografts obtained from surgically resected samples (P13 and P15) and an autopsy sample (P14). As a whole, compared to the isotype control, 7 of 15 HCCs contained definite EpCAM$^+$ cells (46.7%), whereas only 3 HCCs

Address reprint requests to: Taro Yamashita, M.D., Ph.D., Department of General Medicine, Kanazawa University Hospital, 13-1 Takara-Machi, Kanazawa, Ishikawa 920-8641, Japan. E-mail: taroy@m-kanazawa.jp; fax: +81-76-234-4250.

View this article online at wileyonlinelibrary.com.

DOI 10.1002/hep.26168

Potential conflict of interest: Nothing to report.

Additional Supporting Information may be found in the online version of this article.

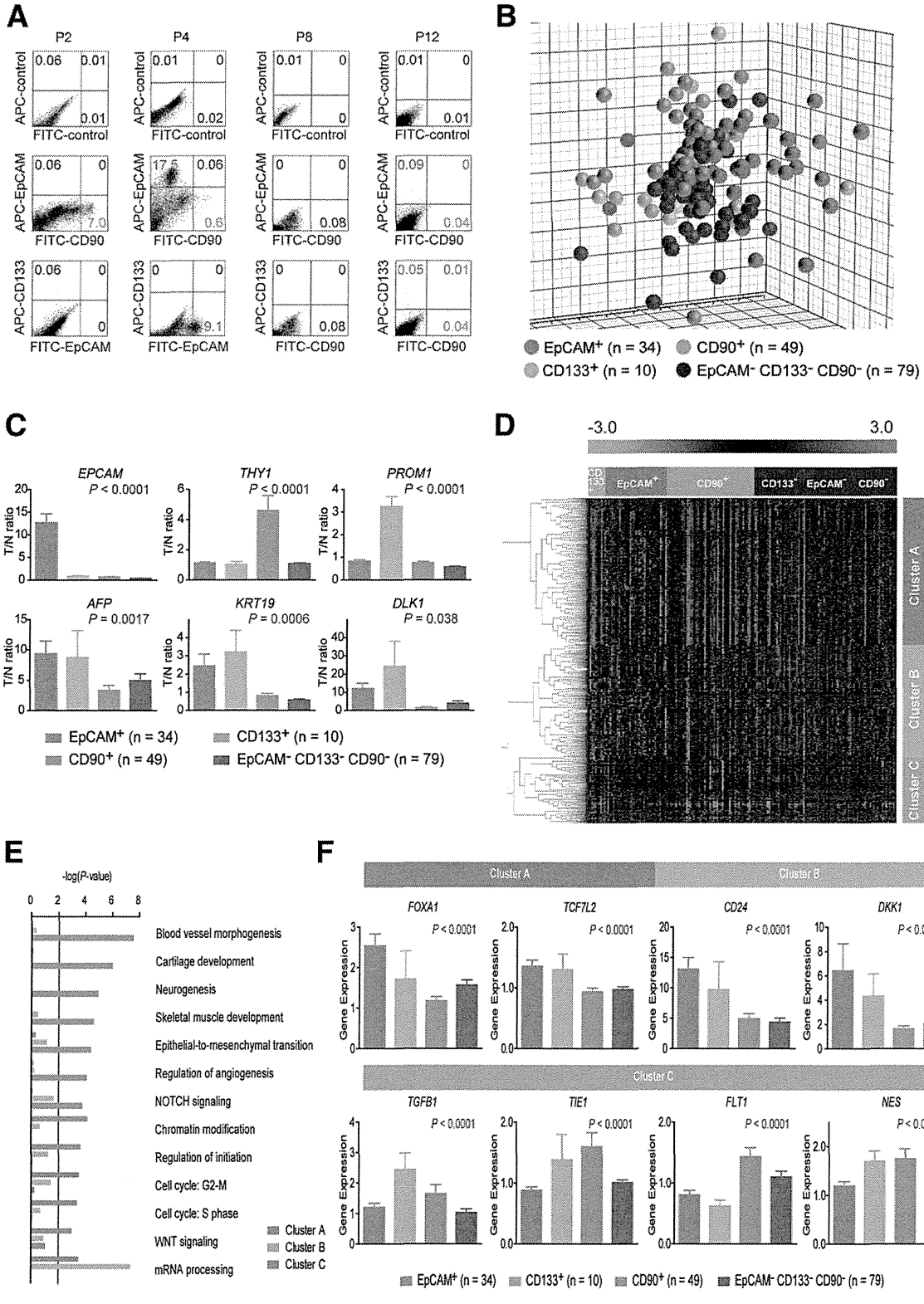

Fig. 1. Gene-expression profiles of CSC marker-positive HCCs. (A) FACS analysis of primary HCCs stained with fluorescent-labeled Abs against EpCAM, CD90, or CD133. (B) Multidimensional scaling analysis of 172 HCC cases characterized by the expression patterns of EpCAM, CD133, and CD90. Red, $EpCAM^+$ $CD90^-$ $CD133^-$ (n = 34); orange, $EpCAM^-$ $CD90^-$ $CD133^+$ (n = 10); light blue, $EpCAM^-$ $CD90^+$ $CD133^-$ (n = 49); blue, $EpCAM^-$ $CD90^-$ $CD133^-$ (n = 79). HCC specimens were clustered in specific groups with statistical significance ($P < 0.001$). (C) Expression patterns of well-known hepatic stem/progenitor markers in each HCC subtype, as analyzed by microarray. Red bar, $EpCAM^+$; orange bar, $CD133^+$; light blue bar, $CD90^+$; blue bar, $EpCAM^-$ $CD90^-$ $CD133^-$. (D) Hierarchical cluster analysis based on 1,561 EpCAM/CD90/CD133-coregulated genes in 172 HCC cases. Each cell in the matrix represents the expression level of a gene in an individual sample. Red and green cells depict high and low expression levels, respectively, as indicated by the scale bar. (E) Pathway analysis of EpCAM/CD90/CD133-coregulated genes. Canonical signaling pathways activated in cluster A (red bar), cluster B (orange bar), or cluster C (light blue bar) with statistical significance ($P < 0.01$) are shown. (F) Expression patterns of representative genes differentially expressed in EpCAM/CD90/CD133 HCC subtypes. Red bar, $EpCAM^+$; orange bar, $CD133^+$; light blue bar, $CD90^+$; blue bar, $EpCAM^-$ $CD133^-$ $CD90^-$.

Table 2. Tumorigenic Capacity of Unsorted, EpCAM$^+$, EpCAM$^-$, CD90$^+$, and CD90$^-$ Cells From Primary HCCs and Xenografts

Sample	CD133 (%)	CD90 (%)	EpCAM (%)	Cell Surface Marker	Number of Cells	Tumor Formation 2M	Tumor Formation 3M
P1	0	3.1	0	Unsorted	1×10^7	0/5	0/5
				CD90$^+$	1×10^5	0/5	0/5
				CD90$^-$	1×10^5	0/5	0/5
P2	0.06	7.0	0.06	Unsorted	1×10^7	0/5	0/5
				CD90$^+$	1×10^5	0/5	0/5
				CD90$^-$	1×10^5	0/5	0/5
P3	0	1.3	0	Unsorted	1×10^6	0/2	0/2
				CD90$^+$	1×10^4	0/4	0/4
				CD90$^-$	1×10^4	0/4	0/4
P4	0	0.6	17.5	Unsorted	1×10^6	3/4	4/4
				EpCAM$^+$	1×10^3	0/3	2/3
					1×10^4	3/4	4/4
					1×10^5	3/3	3/3
				CD90$^+$	1×10^3	0/3	0/3
					1×10^4	0/4	0/4
					1×10^5	0/3	0/3
				EpCAM$^-$ CD90$^-$	1×10^3	0/3	0/3
					1×10^4	0/4	0/4
					1×10^5	0/3	0/3
P5	0	0.8	29.7	Unsorted	1×10^6	0/5	0/5
				EpCAM$^+$	1×10^5	0/5	0/5
				CD90$^+$	1×10^5	0/5	0/5
				EpCAM$^-$ CD90$^-$	1×10^5	0/5	0/5
P6	0	0.7	0	Unsorted	1×10^6	0/2	0/2
				CD90$^+$	1×10^4	0/4	0/4
				CD90$^-$	1×10^4	0/4	0/4
P7	1.38	4.5	4.4	Unsorted	1×10^6	2/2	2/2
				EpCAM$^+$	2×10^2	0/3	0/3
					1×10^3	0/3	1/3
					1×10^4	2/4	4/4
				CD90$^+$	2×10^2	0/3	0/3
					1×10^3	0/3	0/3
					1×10^4	0/4	0/4
				EpCAM$^-$ CD90$^-$	1×10^3	0/3	0/3
					1×10^4	0/3	0/3
					1×10^5	0/4	0/4
P8	0	0.08	0	Unsorted	1×10^5	0/4	0/4
				CD90$^+$	1×10^3	0/3	0/3
				CD90$^-$	1×10^5	0/3	0/3
P9	0	0.26	0	Unsorted	1×10^5	0/4	0/4
				CD90$^+$	1×10^3	0/3	0/3
				CD90$^-$	1×10^5	0/3	0/3
P10	0	0.78	0	Unsorted	1×10^4	0/4	0/4
				CD90$^+$	1×10^3	0/3	0/3
				CD90$^-$	1×10^4	0/3	0/3
P11	0	0.1	1.54	Unsorted	5×10^4	0/2	0/2
				EpCAM$^+$	1×10^3	0/3	0/3
				CD90$^+$	1×10^3	0/3	0/3
				EpCAM$^-$ CD90$^-$	1×10^4	0/3	0/3
P12	0.06	0.05	0.09	Unsorted	1×10^5	0/3	3/3
				CD90$^+$	1×10^3	0/4	1/4
				CD90$^-$	1×10^3	0/4	1/4
					1×10^4	0/3	3/3
P13	0	0.03	67.7	EpCAM$^+$	5×10^5	4/4	NA
					5×10^4	3/3	NA
					5×10^3	3/3	NA
				EpCAM$^-$	5×10^5	0/4	NA
					5×10^4	0/3	NA
					5×10^3	0/3	NA
P14	24.0	0.06	3.1	EpCAM$^+$	5×10^3	4/5	NA
				EpCAM$^-$	5×10^3	2/5	NA
P15	0	2.45	0	CD90$^+$	5×10^4	3/4	NA
					5×10^3	1/3	NA
					5×10^2	1/3	NA
				CD90$^-$	5×10^4	2/4	NA
					5×10^3	1/3	NA
					5×10^2	0/3	NA

NA, not available.

contained definite CD133$^+$ cells (20%) (Table 2). CD90$^+$ cells were detected at variable frequencies in all 15 HCCs analyzed.

To explore the status of these CSC marker-positive cells in HCC in a large cohort, we utilized oligo-DNA microarray data from 238 HCC cases (GEO accession no.: GSE5975) to evaluate the expression of *EPCAM* (encoding EpCAM and CD326), *THY1* (encoding CD90), and *PROM1* (encoding CD133) in whole HCC tissues and nontumor (NT) tissues. Because previous studies demonstrated that CD133$^+$ and CD90$^+$ cells were detected at low frequency (~13.6% by CD133 staining and ~6.2% by CD90 staining) in HCC, but were almost nonexistent in NT liver (4, 5),[4,5] we utilized tumor/nontumor (T/N) gene-expression ratios to detect the existence of marker-positive CSCs in tumor. Accordingly, we showed that a 2-fold cutoff of T/N ratios of *EPCAM* successfully stratifies HCC samples with EpCAM$^+$ liver CSCs.[9,10]

A total of 95 (39.9%), 110 (46.2%), and 31 (13.0%) of the 238 HCC cases were thus regarded as EpCAM$^+$, CD90$^+$, and CD133$^+$ HCCs (T/N ratios: $\geq$2.0), respectively. As observed in the FACS data described above, we detected coexpression of EpCAM and CD90 in 45 HCCs (18.9%), EpCAM and CD133 in five HCCs (2%), CD90 and CD133 in five HCCs (2%), and EpCAM, CD90, and CD133 in 11 HCCs (4.6%). To clarify the characteristics of gene-expression signatures specific to stem cell marker expression status, we selected 172 HCC cases expressing a single CSC marker (34 EpCAM$^+$ CD90$^-$ CD133$^-$, 49 EpCAM$^-$ CD90$^+$ CD133$^-$, and 10 EpCAM$^-$ CD90$^-$ CD133$^+$) or all marker-negative HCCs (79 EpCAM$^-$ CD90$^-$ CD133$^-$). A class-comparison analysis with

univariate F tests and a global permutation test (×10,000) yielded a total of 1,561 differentially expressed genes. Multidimensional scaling (MDS) analysis using this gene set indicated that HCC specimens were clustered in specific groups with statistical significance ($P < 0.001$). Close examination of MDS plots revealed three major HCC subtype clusters: all marker-negative HCCs (blue spheres); EpCAM single-positive HCCs (red spheres); and CD90 single-positive HCCs (light blue spheres). $CD133^+$ HCCs (orange spheres) were rare, relatively scattered, and not clustered (Fig. 1B).

We examined the expression of representative hepatic stem/progenitor cell markers *AFP*, *KRT19*, and *DLK1* in HCCs with regard to the gene-expression status of each CSC marker (Fig. 1C). All three markers were up-regulated in $EpCAM^+$ and $CD133^+$ HCCs, compared with all marker-negative HCCs, consistent with previous findings.[10,11] However, we found no significant overexpression of *AFP*, *KRT19*, and *DLK1* in $CD90^+$ and all marker-negative HCCs.

Hierarchical cluster analyses revealed three main gene clusters that were up-regulated in $EpCAM^+$ HCCs (cluster A, 706 genes), $EpCAM^+$ or $CD133^+$ HCCs (cluster B, 530 genes), and $CD90^+$ or $CD133^+$ HCCs (cluster C, 325 genes) (Fig. 1D). Pathway analysis indicated that the enriched genes in cluster A (red bar) were associated with chromatin modification, cell-cycle regulation, and Wnt/β-catenin signaling (Fig. 1E). Genes associated with messenger RNA processing were enriched in clusters A (red bar) and B (orange bar). Surprisingly, genes in cluster C were significantly associated with pathways involved in blood-vessel morphogenesis, angiogenesis, neurogenesis, and epithelial mesenchymal transition (EMT) (light blue bar). Close examination of genes in each cluster suggested that known hepatic transcription factors (*FOXA1*), Wnt regulators (*TCF7L2* and *DKK1*), and a hepatic stem cell marker (*CD24*) were dominantly up-regulated in $EpCAM^+$ and $CD133^+$ HCCs (Fig. 1F). By contrast, genes associated with blood-vessel morphogenesis (*TIE1* and *FLT1*), EMT (*TGFB1*), and neurogenesis (*NES*) were activated dominantly in $CD90^+$ HCCs and $CD133^+$ HCCs.

$CD90^+$ HCC Cells Share Features With Mesenchymal Vascular Endothelial Cells. Because $CD133^+$ HCCs were relatively rare and constituted only 13% (microarray cohort) to 20% (FACS cohort) of all HCC samples analyzed, we focused on the characterization of EpCAM and CD90. To clarify the cell identity of $EpCAM^+$ or $CD90^+$ cells in primary HCCs, we performed IHC analysis of 18 needle-biopsy specimens of premalignant dysplastic nodules (DNs), 102 surgically resected HCCs, and corresponding NT liver tissues. When examining the expression of EpCAM and CD90 in cirrhotic liver tissue by double-color IHC analysis, we found that $EpCAM^+$ cells and $CD90^+$ cells were distinctively located and not colocalized (Supporting Fig. 1A). Immunoreactivity (IR) to anti-CD90 antibodies (Abs) was detected in vascular endothelial cells (VECs), inflammatory cells, fibroblasts, and neurons, but not in hepatocytes or cholangiocytes, in the cirrhotic liver (Supporting Fig. 1B, panels a,b). IR to anti-EpCAM Abs was detected in hepatic progenitors adjacent to the periportal area and bile duct epithelial cells in liver cirrhosis (Supporting Fig. 1B, panels c,d).

IR to anti-EpCAM Abs was detected in 37 of 102 surgically resected HCCs (Fig. 2A, panel b), but not in 18 DNs (Fig. 2A, panel a). By contrast, no tumor epithelial cells (TECs) showing IR to anti-CD90 Abs were found in any of the 18 DNs or 102 HCCs examined (Fig. 2A, panels c,d). However, we identified $CD90^+$ cells that were morphologically similar to VECs or fibroblasts within the tumor nodule in 37 of the 102 surgically resected HCC tissues (≥5% positive staining in a given area). IR to anti-CD90 Abs was also detected in hepatic mesenchymal tumors (Supporting Fig. 1C, panels a-c), indicating that CD90 is also a marker of liver stromal tumors.

Double-color IHC and immunofluorescence (IF) analysis confirmed the distinct expression of EpCAM and CD90 in HCC (Fig. 2B), consistent with the FACS data (Fig. 1A). Quantitative real-time polymerase chain reaction (qPCR) analysis of sorted $EpCAM^+$, $CD90^+$, and $EpCAM^-$ $CD90^-$ cells after $CD45^+$ cell depletion indicated that the hepatic stem/progenitor markers, *AFP* and *KRT19*, were up-regulated in $EpCAM^+$ cells (red bar), whereas the mesenchymal markers, *KIT* and *FLT1*, were up-regulated in $CD90^+$ cells (orange bar), compared with $EpCAM^-$ $CD90^-$ cells (blue bar) (Fig. 2C). The hepatocyte marker, *CYP3A4*, was down-regulated in $EpCAM^+$ cells and not detected in $CD90^+$ cells, compared with $EpCAM^-$ $CD90^-$ cells. *POU5F1* and *BMI1* were equally up-regulated in both $EpCAM^+$ and $CD90^+$ cells, compared with $EpCAM^-$ $CD90^-$ cells.

EpCAM and CD90 were independently and distinctively expressed in different cellular lineages, so we evaluated the staining of EpCAM and CD90 separately and analyzed the clinicopathological characteristics of surgically resected HCC cases. HCCs were regarded marker positive if ≥5% positive staining was detected in a given area. The existence of $EpCAM^+$

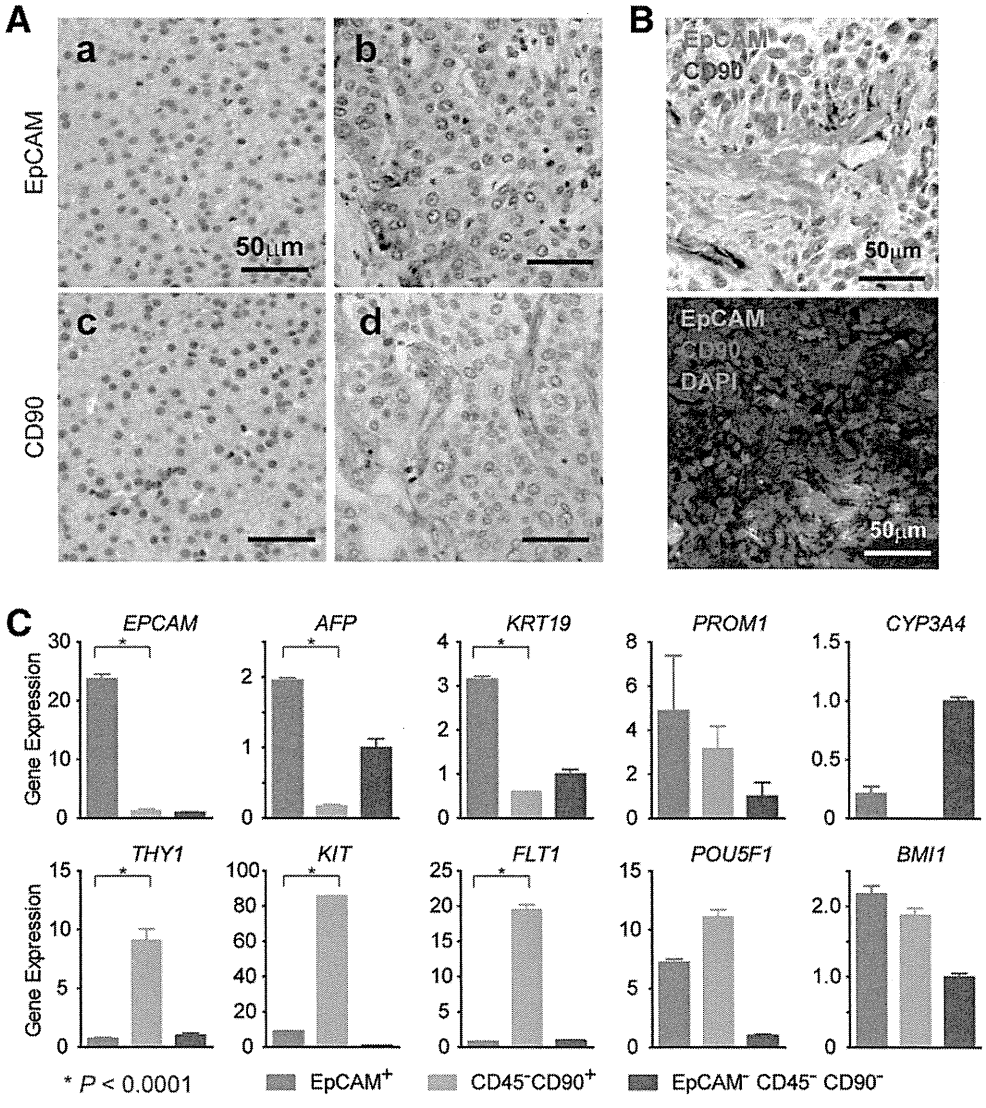

Fig. 2. Distinct EpCAM$^+$ and CD90$^+$ cell populations in HCC. (A) Representative images of EpCAM and CD90 staining in dysplastic nodule (panels a,c) and HCC (panels b,d) by IHC analysis (scale bar, 50 μm). EpCAM (panels a,b) and CD90 (panels c,d) immunostaining is depicted. (B) Upper panel: representative images of EpCAM (red) and CD90 (brown) double staining in HCC by IHC (scale bar, 50 μm). Lower panel: representative images of EpCAM (green) and CD90 (red) staining with 4'6-diamidino-phenylindole (DAPI) (blue) in HCC by IF (scale bar, 50 μm). (C) qPCR analysis of sorted EpCAM$^+$ (red bar), CD90$^+$ (orange bar), or EpCAM$^-$ CD90$^-$ (blue bar) derived from a representative primary HCC. Experiments were performed in triplicate, and data are shown as mean ± standard error of the mean.

cells (≥5%) was characterized by poorly differentiated morphology and high serum AFP values with a tendency for portal vein invasion, whereas the existence of CD90$^+$ cells (≥5%) was associated with poorly differentiated morphology and a tendency for large tumor size (Supporting Tables 2 and 3). Notably, the existence of CD90$^+$ cells was associated with a high incidence of distant organ metastasis, including lung, bone, and adrenal gland, within 2 years after surgery, whereas EpCAM$^+$ cell abundance appeared unrelated to distant organ metastasis.

We evaluated the characteristics of EpCAM$^+$ or CD90$^+$ cells in seven representative HCC cell lines. Morphologically, all EpCAM$^+$ cell lines (HuH1, HuH7, and Hep3B) showed a polygonal, epithelial cell shape, whereas three of four CD90$^+$ cell lines (HLE, HLF, and SK-Hep-1) showed a spindle cell shape (Fig. 3A). EpCAM$^+$ cells were detected in 11.5%, 57.7%, and 99.6% of sorted HuH1, HuH7, and Hep3B cells, respectively. A small CD90$^+$ cell population (0.66%) was observed in PLC/PRL/5, whereas 91.3%, 10.8%, and 59.0% of CD90$^+$ cells were detected in HLE, HLF, and SK-Hep-1, respectively. Compared with primary HCCs, only EpCAM$^+$ or CD90$^+$ cells were detected in liver cancer cell lines under normal culture conditions (Fig. 3B), suggesting that these cell lines contain a relatively pure cell population most likely obtained by clonal selection through the establishment process.

A class-comparison analysis with univariate t tests and a global permutation test (×10,000) of microarray data yielded two main gene clusters up-regulated in EpCAM$^+$ cell lines (HuH1, HuH7, and Hep3B) (cluster I, 524 genes) or in CD90$^+$ cell lines (HLE, HLF, and SK-Hep-1) (cluster II, 366 genes) (Fig. 3C). PLC/PRL/5 showed intermediate gene-expression patterns between EpCAM$^+$ and CD90$^+$ cell lines using this gene set. Pathway analysis indicated that the genes

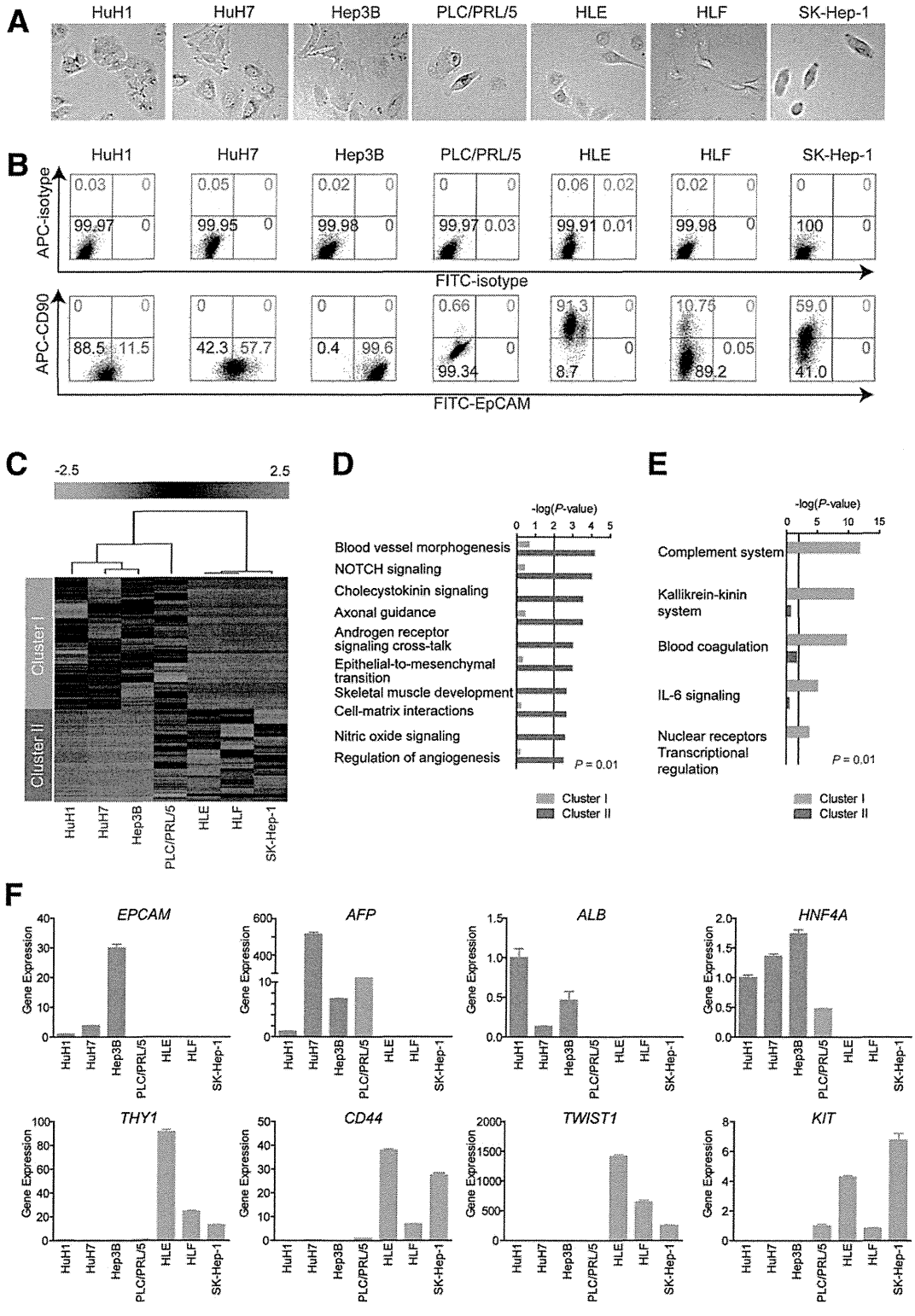

Fig. 3. Characteristics of HCC cell lines defined by EpCAM and CD90. (A) Representative photomicrographs of $EpCAM^{+}CD90^{-}$ and $EpCAM^{-}CD90^{+}$ HCC cell lines. (B) Representative FACS data of $EpCAM^{+}CD90^{-}$ and $EpCAM^{-}$ $CD90^{+}$ HCC cell lines stained with fluorescein isothiocyanate (FITC)-EpCAM and APC-CD90 Abs. (C) Heat-map images of seven HCC cell lines based on 890 EpCAM/CD90-coregulated genes. Each cell in the matrix represents the expression level of a gene in an individual sample. Red and green cells depict high and low expression levels, respectively, as indicated by the scale bar. (D and E) Pathway analysis of EpCAM/CD90-coregulated genes. Canonical signaling pathways activated in cluster I (orange bar) or II (blue bar) with statistical significance ($P < 0.01$) are shown. (F) qPCR of representative differentially expressed genes identified by microarray analysis (C) in seven HCC cell lines.

enriched in cluster II were mainly associated with blood-vessel morpho- and angiogenesis (Fig. 3D). By contrast, the enriched genes in cluster I were significantly associated with known hepatocyte functions ($P < 0.01$) (Fig. 3E). In addition, we identified that the enriched genes in cluster II were significantly associated with neurogenesis, skeletal muscle development, and EMT.

We used qPCR to validate that known hepatic stem cell (HSC) and hepatocyte markers, such as *AFP*, *EPCAM*, *ALB*, and *HNF4A* genes, were up-regulated in $EpCAM^+$ cell lines, but not detected in $CD90^+$ cell lines (Fig. 3F). By contrast, genes associated with mesenchymal lineages and EMT, such as *KIT*, *TWIST1*, *CD44*, and *THY1*, were strongly up-regulated in $CD90^+$ cell lines.

Unique Tumorigenicity and Metastasis Capacity of Distinct CSCs Defined by EpCAM and CD90. We investigated the tumorigenic capacity of $EpCAM^+$ or $CD90^+$ cells by subcutaneously (SC) injecting 1×10^5 sorted cells of four HCC cell lines (HuH1, HuH7, HLE, and HLF) into nonobese diabetic, severe combined immunodeficient (NOD/SCID) mice. We excluded Hep3B cells for the evaluation of tumorigenicity because almost 100% of cells were EpCAM positive. We further excluded SK-Hep-1 cells from the analysis because they potentially originated from endothelial cells.[12] The highly tumorigenic capacities of $EpCAM^+$ and $CD90^+$ cells were reproduced in HuH1, HuH7, and HLF cell lines, compared with marker-negative cells (Fig. 4A). However, HLE cells did not produce SC tumors, even 12 months after transplantation, in NOD/SCID mice. $EpCAM^+$ cells from HuH1 and HuH7 formed larger tumors more rapidly than $CD90^+$ cells from HLF (Fig. 4B). IHC analyses indicated that $EpCAM^+$ cells did not produce $CD90^+$ cells and *vice versa* in these cell lines *in vivo* (Fig. 4C). $CD90^+$ cells showed a high metastatic capacity, whereas $EpCAM^+$ cells showed no metastasis to the lung when SC tumor volume reached approximately 2,000 (HuH1 and HuH7) or 700 mm^3 (HLF) (Fig. 4D). The high metastatic capacity of PLC/PRL/5 cells, which contain a small population of $CD90^+$ cells, was also confirmed after SC injection into NOD/SCID mice (data not shown). $CD90^+$ cells could divide to generate both $CD90^+$ and $CD90^-$ cells, and $CD90^+$ cells showed a high capacity to invade and form spheroids with overexpression of *TWIST1* and *TWIST2*, which are known to activate EMT programs in HLF cells (Supporting Fig. 2A-D).

We next evaluated the tumorigenic/metastatic capacity of $CD45^-$ tumor cells using 12 fresh primary HCC specimens (P1-P12) that had been surgically resected (Table 2). We further evaluated the tumorigenicity of EpCAM/CD90 sorted cells obtained from xenografts derived from primary HCCs (Supporting Fig. 3A). Of these, we confirmed the tumorigenicity of cancer cells obtained from six primary HCCs after SC injection into NOD/SCID mice within 3 months after transplantation (Fig. 5A; Table 2; Supporting Fig. 3B). $EpCAM^+$ cells derived from four HCCs (P4, P7, P13, and P14) showed highly tumorigenic capacities, compared with $EpCAM^-$ cells. $CD90^+$ cells derived from two HCCs showed equal (P12) or more-tumorigenic capacities (P15), compared with $CD90^-$ cells. Tumorigenicity of $EpCAM^+$ cells was observed in three hepatitis C virus (HCV)-related HCCs and an hepatitis B virus (HBV)-related HCC, whereas tumorigenicity of $CD90^+$ cells was observed in two HBV-related HCCs (Tables 1 and 2).

Using unsorted cells, we compared the frequency of $EpCAM^+$ and $CD90^+$ cells in primary and xenograft tumors and found that $EpCAM^+$ cells remained, but $CD90^+$ cells disappeared, in secondary tumors derived from P4 or P7, whereas $EpCAM^+$ cells disappeared, but $CD90^+$ cells remained, in secondary tumors derived from P12 (Fig. 5B). Morphologically, tumorigenic $EpCAM^+$ cells showed an epithelial cell shape, whereas $CD90^+$ cells showed a mesenchymal VEC shape (Fig. 5C and Supporting Fig. 3C). FACS analysis indicated that P12 HCC cells showed abundant expression of vascular endothelial growth factor receptor (VEGFR) 1 and a vascular endothelial marker endoglin (CD105) (Fig. 5D). By contrast, P4 and P7 HCC cells did not express these vascular endothelial markers (data not shown). Lung metastasis was detected in NOD/SCID mice transplanted with P12 HCC cells, but not in mice transplanted with P4 and P7 HCC cells (Fig. 5E,F).

Taken together, these results suggest that the tumorigenic and metastatic capability of primary HCC may depend on the presence of distinct $EpCAM^+$ or $CD90^+$ CSCs. $EpCAM^+$ cells were associated with a high tumorigenic capacity with hepatic epithelial stem cell features, whereas $CD90^+$ cells were related to the metastatic propensity with VEC features.

Suppression of Lung Metastasis Mediated by $CD90^+$ CSCs by Imatinib Mesylate. We previously demonstrated that Wnt/β-catenin signaling inhibitors could successfully attenuate the tumorigenic capacity of $EpCAM^+$ CSCs in HCC.[8,10] To explore the potential molecular targets activated in $CD90^+$ CSCs, we investigated the expression of the known VEC markers, CD105, VEGFR1 (encoded by *FLT1*), and

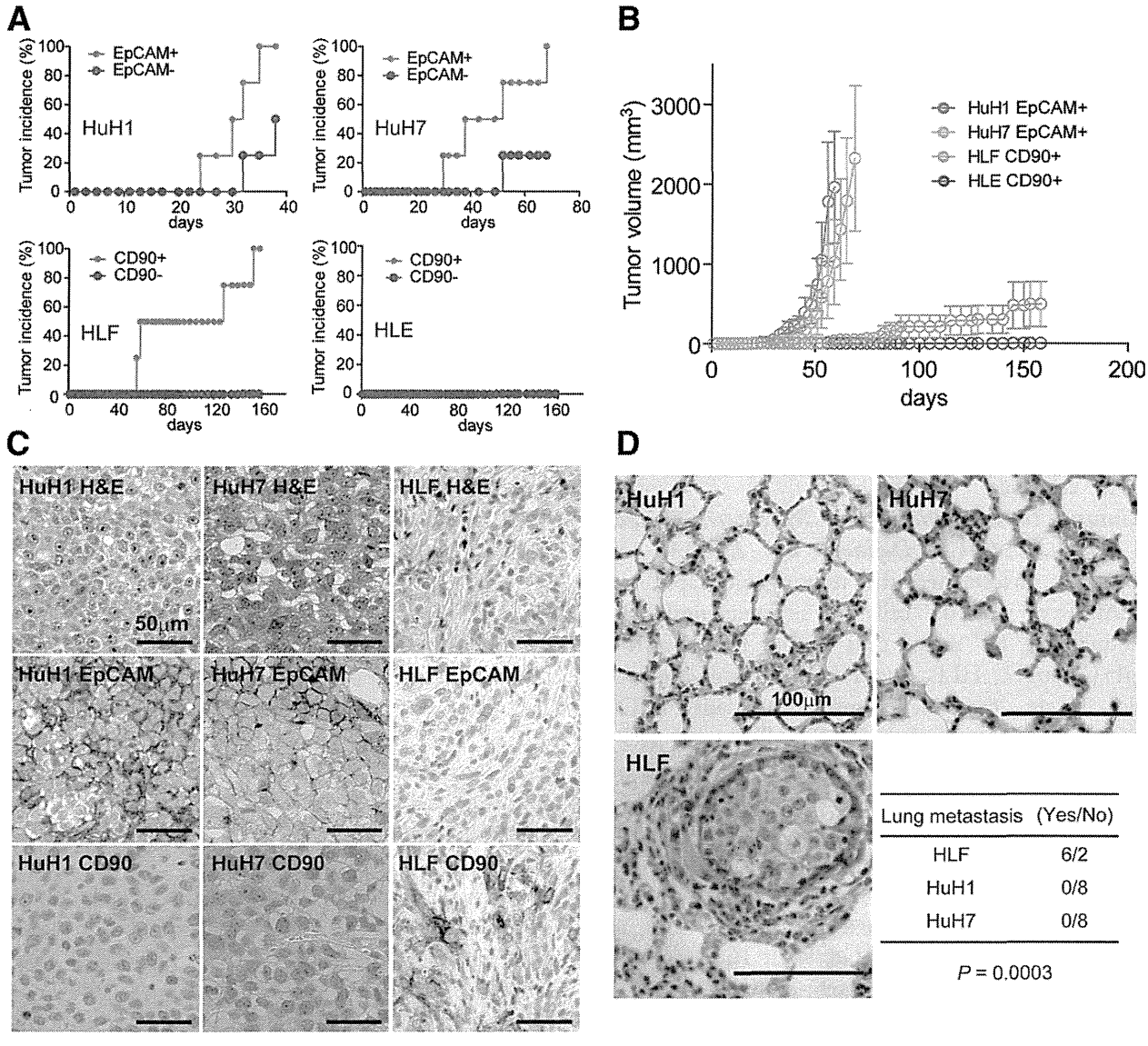

Fig. 4. Distinct tumorigenic/metastatic capacities of HCC cell lines defined by EpCAM and CD90. (A) Tumorigenicity of 1×10^5 cells sorted by anti-EpCAM (HuH1 and HuH7) or anti-CD90 (HLE and HLF) Abs. Data are generated from 8 mice/cell line. (B) Tumorigenic ability of $EpCAM^+$ and $CD90^+$ sorted cells in NOD/SCID mice. Aggressive tumor growth in the SC lesion was observed in $EpCAM^+$ HuH1 or HuH7 cells, compared with $CD90^+$ HLE or HLF cells. $EpCAM^+$ (1×10^5) or $CD90^+$ cells were injected. Tumor-volume curves are depicted as mean ± standard deviation of 4 mice/group. (C) Histological analysis of $EpCAM^+$ or $CD90^+$ cell-derived xenografts. Hematoxylin and eosin (H&E) staining of a SC tumor (upper panels) and IHC of the tumor with anti-EpCAM (middle panels) or anti-CD90 Abs (bottom panels) are shown (scale bar, 50 μm). (D) Metastasis was evaluated macroscopically and microscopically in the left and right lobes of the lung separately in each mouse (n = 4) (scale bar, 100 μm).

c-Kit (encoded by *KIT*), in cell lines and showed that they were abundantly expressed in $CD90^+$ cell lines, but not $EpCAM^+$ cell lines (Fig. 6A). No expression of VEGFR2 was detected in this set of cell lines, suggesting that molecular reagents specifically targeting VEGFR2 may have no effects on $CD90^+$ CSCs. CD44, a stem cell marker that functionally regulates redox status and is a potential target of $CD90^+$ CSCs, was also abundantly expressed in $CD90^+$ cell lines (Supporting Fig. 4A), consistent with previous data.[5,13] No significant difference was detected in the expression of the hematopoietic marker, CD34, or ABCG2 between $EpCAM^+$ and $CD90^+$ cell lines (Supporting Fig. 4A).

Among these molecular targets, we focused on the characterization of c-Kit because the c-Kit tyrosine kinase inhibitor, imatinib mesylate, is readily available, is widely used for the treatment of gastrointestinal stromal tumor with activation of c-Kit, and may have potential antitumor activity against a subset of HCC.[14] We explored the effect of imatinib mesylate on HCC cell lines and found that treatment with 10

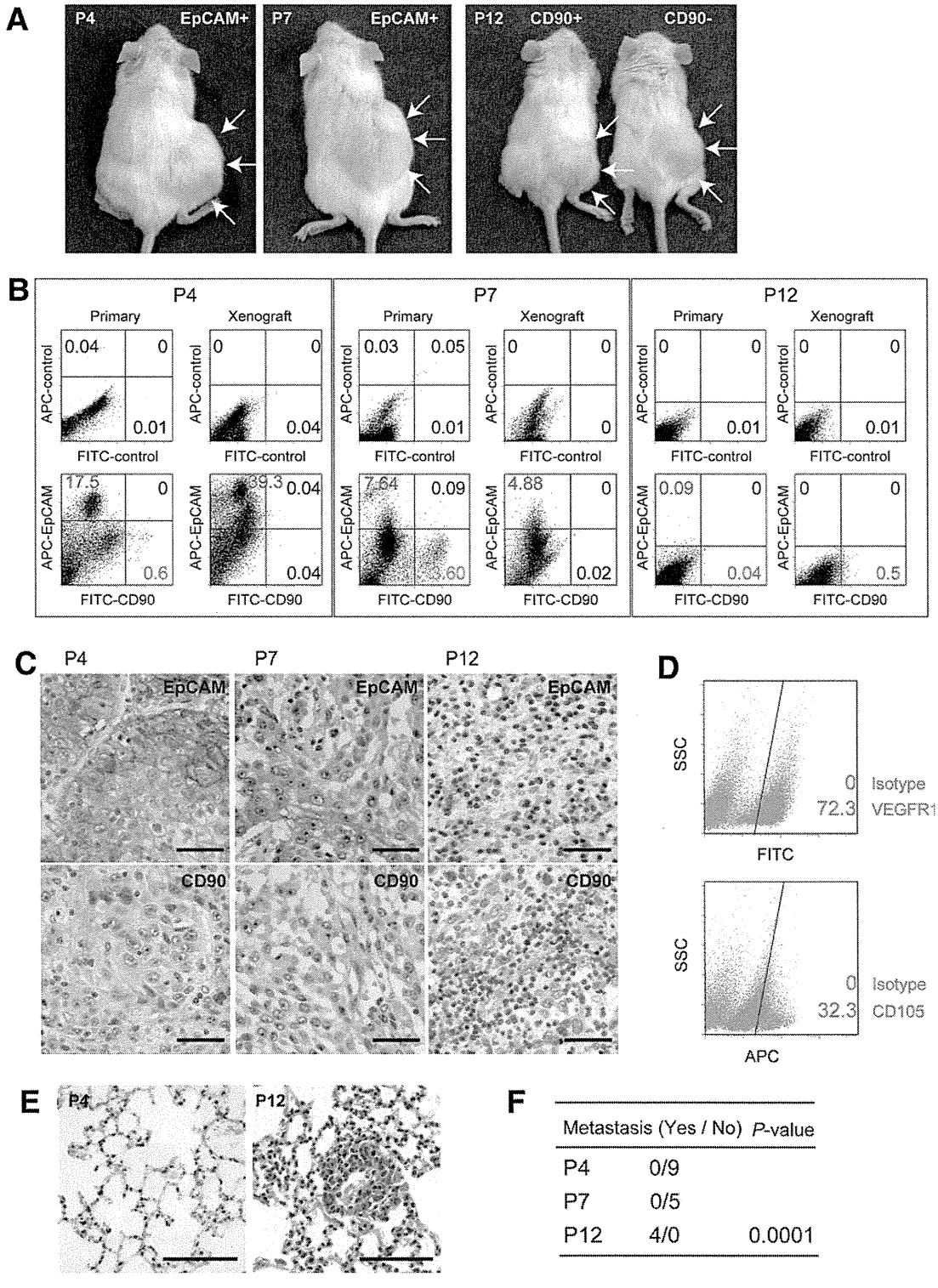

Fig. 5. Tumorigenic/metastatic capacities of EpCAM$^+$ and CD90$^+$ cells in primary HCC. (A) Representative NOD/SCID mice with SC tumors (white arrows) from EpCAM$^+$ P4 or P7 cells (left and middle panels) and CD90$^+$ or CD90$^-$ P12 cells (right panel). (B) FACS analysis of CD90 and EpCAM staining in primary HCCs and the corresponding secondary tumors developed in NOD/SCID mice. Unsorted cells (1×10^6 cells in P4 and P7 or 1×10^5 cells in P12) were SC injected to evaluate the frequency of each marker-positive cell in primary and secondary tumors. (C) IHC analysis of EpCAM and CD90 in primary HCCs P4, P7, and P12 (scale bar, 50 μm). (D) FACS analysis of VEGFR1 (Alexa488) and CD105 (APC) in primary HCC P12. (E) Hematoxylin and eosin staining of lung tissues in P4 and P12 (scale bar, 200 μm). (F) Frequency of lung metastasis in NOD/SCID mice SC transplanted using unsorted primary HCC cells.

μM reduced cell proliferation and spheroid formation in CD90$^+$ cell lines, but had no effect on EpCAM$^+$ cell lines (Supporting Fig. S4B,C).

We further explored the effect of imatinib mesylate *in vivo*. Because EpCAM$^+$ and CD90$^+$ cells reside in the primary HCC, but not in established cell lines, we SC injected HuH7 and HLF cell lines to generate tumors organized by EpCAM$^+$ and CD90$^+$ CSCs. Interestingly, when HLF cells were coinjected with HuH7 cells, EpCAM$^+$ cells could metastasize to the lung, whereas

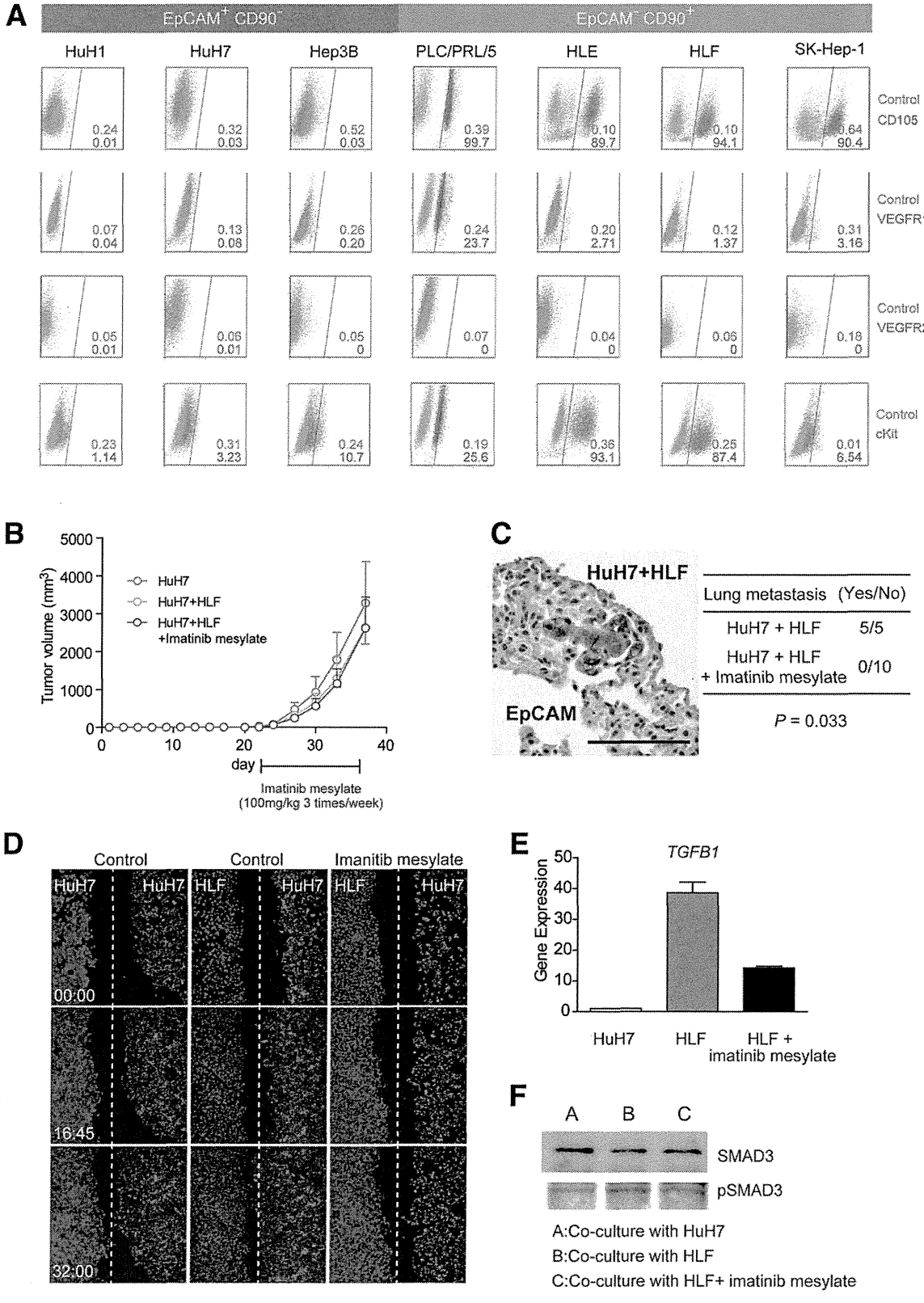

Fig. 6.

SC primary tumors showed no difference in size (Fig. 6B,C). Furthermore, although imatinib mesylate treatment had little effect on the size of primary SC tumors, it significantly suppressed lung metastasis in primary tumors (Fig. 6C). These data suggest that $CD90^+$ cells are not only metastatic to the distant organ, but also help the metastasis of $CD90^-$ cells, including $EpCAM^+$ cells, which originally have no distant metastatic capacity. Our data further suggest that imatinib mesylate can inhibit distant organ metastasis by suppressing $CD90^+$ metastatic CSCs, albeit with little effect on $EpCAM^+$ tumorigenic epithelial stem-like CSCs.

To explore the potential mechanism of how $CD90^+$ cells dictate the metastasis of $EpCAM^+$ cells, we utilized coculture systems and time-lapse image analysis. Wound-healing analysis clearly indicated that motility of HuH7 cells was enhanced when HLF cells were cocultured, and this effect was abolished by imatinib mesylate treatment (Fig. 6D; see Supporting Videos 1-3). HLF cells abundantly expressed *TGFB1*, compared with HuH7 cells, and its expression was dramatically suppressed by imatinib mesylate treatment (Fig. 6E). Mothers against decapentaplegic homolog 3 (Smad3) phosphorylation was augmented in HuH7 cells when cocultured with HLF cells, and this effect was attenuated when cocultured with HLF cells pretreated with imatinib mesylate.

Taken together, our data suggest that liver CSCs are not a single entity. Liver CSCs defined by different markers show unique features of tumorigenicity/metastasis with phenotypes closely associated with committed liver lineages. These distinct CSCs may collaborate to enhance tumorigenicity and metastasis of HCCs.

Discussion

The current investigation demonstrates that CSC marker expression status may be a key determinant of cancer phenotypes, in terms of metastatic propensity and chemosensitivity, to certain molecularly targeted therapies. EpCAM appears to be an epithelial tumorigenic CSC marker, whereas CD90 seems to be a mesenchymal metastatic CSC marker associated with expression of c-Kit and chemosensitivity to imatinib mesylate. Imatinib mesylate may be effective in inhibiting metastasis, but has little effect on primary $EpCAM^+$ HCC cell growth.

We investigated the frequency of three CSC markers (EpCAM, CD90, and CD133) in 15 primary HCCs with a confirmed cell viability of $\geq$70% and found that three HCCs contained $CD133^+$ cells, seven HCCs contained $EpCAM^+$ cells, and all HCCs contained $CD90^+$ cells. Among them, we confirmed the perpetuation of $CD133^+$ cells derived from three HCCs (P7, P12, and P14; data not shown), $EpCAM^+$ cells derived from four HCCs (P4, P7, P13, and P14), and $CD90^+$ cells derived from two HCCs (P12 and P15). Recent studies showed that at least 8 of 21 HCCs (38%)[4] and 13 of 13 HCCs (100%)[5] contained tumorigenic $CD133^+$ or $CD90^+$ CSCs, respectively. Recent IHC and tissue microarray studies also demonstrated that $CD133^+$ and $CD90^+$ cells were detected in 24.8% ($\geq$1% of tumor cells) and 32.2% ($\geq$5% of tumor cells) of HCC cases examined, respectively.[15,16]

One possible explanation of the comparatively low frequency of $CD133^+$ liver CSCs identified in our study is that we used the monoclonal Ab CD133/2, whereas Ma et al. used CD133/1. Another possible explanation is the difference of etiology related to hepatocarcinogenesis. We examined tumorigenicity using 15 HCCs (five HBV related, four HCV related, three non-B, non-C hepatitis [NBNC] related, and three alcohol related) and identified that tumorigenic CSCs were only obtained from HBV- or HCV-related cases. Previous liver CSC studies were performed using HBV-related HCCs,[4,5] and a recent study showed that

Fig. 6. Suppression of lung metastasis mediated by $CD90^+$ CSCs by imatinib mesylate. (A) FACS analysis of seven HCC cell lines stained by APC-CD105, Alexa 488/VEGFR1, APC/VEGFR2, and Alexa 488/c-Kit Abs or isotype control. (B) Tumorigenicity of 5×10^5 HuH7 cells and 2.5×10^5 HuH7 cells plus 2.5×10^5 HLF cells treated with imatinib mesylate or control phosphate-buffered saline (PBS) (200 μL/mouse) orally ingested three times per week (100 mg/kg) for 2 weeks. Data are generated from 5 mice per condition. (C) IHC analysis of EpCAM in lung metastasis detected in NOD/SCID mice SC injected with 2.5×10^5 HuH7 cells and 2.5×10^5 HLF cells. Metastasis was evaluated macro- and microscopically in the left and right lobes of the lung separately in each mouse ($n = 5$) (scale bar, 100 μm). (D) Cell motility of HuH7 cells cocultured with HuH7, HLF, or HLF cells with imatinib mesylate (10 μM) was monitored in a real-time manner by time-lapse image analysis. HuH7 and HLF cells were labeled with the lipophilic fluorescence tracer, DiI (indicated as red) or DiD (indicated as blue), and incubated in a μ-Slide eight-well chamber overnight. Silicone inserts were detached and the culture media replaced with Dulbecco's modified Eagle's medium containing 10% fetal bovine serum, including 0.1% dimethyl sulfoxide (DMSO) (control) or 10 μM of imatinib mesylate dissolved in DMSO (final concentration 0.1%). Immediately after the medium change, cells were cultured at 37°C in 5% CO_2 and time-lapse images were captured for 72 hours. (E) qPCR analysis of *TGFB1* in HuH7 (white bar), HLF (gray bar), and HLF cells pretreated with imatinib mesylate for 24 hours. (F) Smad3 and its phosphorylation evaluated by western blotting. HuH7 cells and HLF cells were harvested in cell culture inserts and treated with DMSO (0.1%) or imatinib mesylate (10 μM) for 24 hours. Cell culture inserts were washed with PBS, cocultured with HuH7 cells for 8 hours, and then removed. HuH7 cells were lysed using radioimmunoprecipitation assay buffer for western blotting. (A) HuH7 cells cocultured with HuH7 cells. (B) HuH7 cells cocultured with HLF cells. (C) HuH7 cells cocultured with HLF cells pretreated with imatinib mesylate.